RESEARCH

Intensity Prediction Equations for Himalaya and its sub-regions based on data from traditional sources and USGS's Did You Feel It? (DYFI)

P. Anbazhagan · Harish Thakur

Abstract This study has developed Intensity Prediction Equations (IPEs) for the Himalayas and its sub-regions (divided into North-West Himalaya, Central Himalaya, and North-East Himalaya). For this purpose, intensity data reported in previous studies using traditional methods (like field surveys, media reports, and newspapers) and internet-based questionnaires (such as USGS's Did You Feel It? or DYFI) were used to catalogue two separate intensity datasets. Intensities of traditional datasets were also reassessed for some earthquake events by different studies in the different scales of assignment, which was homogenized for the same intensity scale. IPEs are derived for both datasets separately using a two-stage and one-stage regression technique. These IPEs are developed for a first- and second-order relation with respect to earthquake magnitude. A "maximum intensity vs. magnitude approximation of the IPE"

approach relying on an optimal hypocentral depth has also been proposed to select the best-suited IPEs. The information-theoretic approach-based Log-likelihood method (Scherbaum et al. 2009) has been used to check and compare developed IPE performance for events not used for IPE development. These newly developed equations can be used to assess the damage potential of future earthquakes.

Keywords Earthquake · Damages · Maximum intensity · Intensity prediction · Predictive equation · DYFI

1 Introduction

The Himalayan region lies between the Indian and Eurasian continental plates, forming a convergent boundary and the world's largest active thrust fault system. It is a part of the Alpine-Himalayan Orogenic belt (or the Tethyan Orogenic belt), extending more than 15,000 km (Storetvedt 1990). Its boundary on the western end is the Chaman fault system (a transform boundary of more than 850 km) between the Indian plate and the Helmand Block of the Eurasian Plate in a slightly inclined north–south direction. The Eastern end of the region is in Myanmar, marked by the Sagaing fault lying on a transform boundary between the Indian plate and the Sunda plate (Yeats 2012). Major faults present in the region are of reverse slip type found throughout the Himalayan region, along

Highlights
• Updated Intensity Prediction Equations for Himalayas and its sub-regions using a larger dataset.
• New USGS's DYFI-based Intensity Prediction Equations (IPEs) for the region.
• Criteria for optimal hypocentral depth for maximum earthquake intensity/epicentral intensity estimation.

P. Anbazhagan (✉) · H. Thakur
Department of Civil Engineering, Indian Institute of Science, Bengaluru 560012, India
e-mail: anbazhagan@iisc.ac.in

H. Thakur
e-mail: harishthakur@iisc.ac.in

with strike-slip faults in the Indo-Burmese region. This region is covered with Quaternary sediments of Himalayan origin, forming the Indo-Gangetic plains with sedimentary deposits of thickness greater than 8 km (Singh et al. 2015). The Indian and Eurasian plates converge at a relative rate of 40–50 mm/yr, the primary cause of the central Himalayan region's seismicity (Turner et al. 2013). Seismicity in the eastern end of the Himalayas has been attributed to the relative movement of the Indian plate (about 35 mm/yr) with respect to (w.r.t.) the Sunda plate (Socquet et al. 2006). Major earthquake events in the Himalayan region include 1905 M_w 7.5 Kangra, 1934 M_w 8.1 Bihar, 1950 M_w 8.6 Assam, 2005 M_w 7.6 Kashmir, and 2015 M_w 7.8 Nepal earthquakes.

As per Indian code IS 1893 (Part 1): 2016 Seismic Zonation Map of India, most of Northern India falls in Zones III and IV, with some parts lying in Zone V, while the whole of North-East India is under Zone V. As per the code, the Zones III, IV, and V correspond to 1964 Medvedev-Sponheuer-Karnik scale's (or MSK-64) Intensities VII, VIII, and IX (and above). Maximum shaking intensity maps prepared by Martin and Szeliga (2010) based on the macroseismic observations from the past earthquakes (year 1636–2009) also show the occurrence of most damaging intensities being located in the higher zones of the Indian code. This correspondence of the region with high-intensity values highlights the severity of the hazard possible in the Himalayan region. As the population and infrastructure multiply, future earthquake hazards can cause devastating effects on a developing country like India, with considerable tectonically active faults and seismic devastation, as evidenced in several Himalayan earthquakes in the last few decades (Kayal 2008). The empirical fatality model developed by Jaiswal et al. (2009) for India indicates a rate of 1 death per 25 people exposed to shaking Intensity IX and 1 death per 5250 people exposed to Intensity VII. As the population rises, there is a high possibility of intensity even for moderate earthquakes due to vulnerable infrastructure; these estimates are supposed to increase several folds for a future earthquake.

From the point of view of strong-motion station coverage, the Himalayan region has a comparatively smaller number of stations than similarly active regions (e.g., California, Japan, and the Italian peninsula). For the Himalayan region, only a few recently developed Ground Motion Prediction Equations

(GMPEs) are available for a wide range of earthquake magnitudes and distances but not for different soil sites (Anbazhagan et al. 2019). Also, there is no seismic damage or risk prediction model for India even though India has very high seismic exposure and risk as per the global model. In such a scenario, macroseismic intensity data available for the region becomes invaluable for making an impact assessment of the earthquakes. In the absence of GMPEs (based on instrumentally recorded data), these intensity values become necessary for preliminary seismic hazard estimation and effective response against it during an earthquake.

This study aims to develop Intensity Prediction Equations (IPEs) for the Himalayas and its sub-regions, which will be useful for assessing the risk potential of future earthquakes. For this purpose, intensity data available through two different modes (traditional surveys and online sources) is utilized separately. We have also attempted to assess the prediction results from the developed IPEs (based on the two modes) to show how they may lead to different risk/intensity estimates.

1.1 Intensity Prediction Equations (IPEs)

Macroseismic intensity indicates the strength of shaking for an earthquake in any area, unlike instrumental ground motions recorded after an earthquake associated with hazards at a particular location. Intensity data have been used for the development of IPEs (e.g., Atkinson and Wald 2007; Martin and Szeliga 2010) and Ground-motion to Intensity Conversion Equations (GMICEs) (e.g., Wu et al. 2003; Du et al. 2018; Cramer 2020). IPE for a specific earthquake gives attenuation of intensity (I) w.r.t. a distance metric such as epicentral (R_{epi}) or hypocentral distance (R_{hyp}). IPEs developed for a region have been used to constrain historical pre-instrumental earthquakes' magnitude and epicentral location (Musson 1996; Szeliga et al. 2010; Martin and Hough 2015). In the past, reported intensity values have also been used to calibrate conventional hazard probabilistic studies (Mucciarelli et al. 2000). IPE-predicted results have also been used for planning macroseismic surveys after significant events (Musson 2005). Previously done studies for the development of IPEs for the

Table 1 List of IPEs developed (along with the designation) for the Himalayas and its sub-regions from past studies

S. No	Intensity Prediction Equation (IPE)	Events	Relevant region	IPE's abbrev	Reference
1	$I(R_{epi}) - I_0 = 3.975 - 0.001R_{epi} - 3.055\log(R_{epi} + 20)$	3	North-west Himalaya	NWH80	Chandra (1980)
2	$I(R_{epi}) - I_0 = 3.470 - 0.0021R_{epi} - 2.667\log(R_{epi} + 20)$	1	Ganga Basin	GB80	
3	$I(R_{epi}) - I_0 = 2.501 - 0.00452R_{epi} - 1.922\log(R_{epi} + 20)$	4	North-east Himalaya	NEH80	
4	$I = 0.46 + 1.54M_s - 0.004R - 2.54\log_{10}R$	23	Himalayan Region	A&D04	Ambraseys and Douglas (2004)
5	$I = 6.05 + 1.11M_w - 0.0006R_{hyp} - 3.91\log_{10}R_{hyp}$	12	Himalaya	Sze10	Szeliga et al. (2010)
6	$I(R, M_s) = 2.856 + 1.31M_s - 0.0017R_{epi} - 0.9598\ln R_{epi}$	10	North-west Himalaya	G&M11	Ghosh and Mahajan (2011)
7	$I = I_0 + 0.43968 - 0.00017R_{epi} - 0.80248\ln R_{epi}$ $I = 1.4838 + 1.1313M_s - 0.00017R_{epi} - 0.80248\ln R_{epi}$	10	North-west Himalaya	G&M13	Ghosh and Mahajan (2013)
8	$I = 6.32 - 0.004R - 0.815\log R$	1	North-west Himalaya	NWH13	Gupta et al. (2013)
9	$I = 4.78 + 1.14M_w + 2.24R + 0.0027\log R$	5	Sikkim Himalaya	SH13	Prajapati et al. (2013)
10	$I = 8.6757 - 0.0078R_{hyp} - 0.3623\log R_{hyp}$	1	North-east Himalaya	NEH21	Bharali et al. (2021)

R_{epi} epicentral distance, I_0 epicentral intensity, R_{hyp} hypocentral distance, M_s surface wave magnitude, M_w moment magnitude

Himalayan region (Table 1) can be divided into two types, which are as follows:

> 1. IPEs derived from single or multiple earthquake events applicable for *a sub-region of Himalaya*, e.g., Chandra 1980; Ghosh and Mahajan 2011; Ghosh and Mahajan 2013; Prajapati et al. 2013; Bharali et al. 2021.
> 2. IPEs derived from multiple earthquake events applicable to *the Himalayan region*, e.g., Ambraseys and Douglas 2004; Szeliga et al. 2010.

These IPEs are developed by regression analyses using the observed intensity values and associated magnitude and distance parameters. These relations are approximate and keep changing as new data becomes available. IPEs need to be updated after significant earthquake events in a particular region to get better prediction results (Boore and Joyner 1982, for France—Bakun and Scotti 2006, Baumont et al. 2018; for Italy—Gasperini 2001, Pasolini et al. 2008a, 2008b, Gomez-Capera et al. 2023; for UK—Musson 2005, 2013; for Turkey—Sørensen et al. 2009, Bayrak et al. 2019; for Iran—Zare M 2017, Ahmadzadeh et al. 2020). The development of the IPEs requires choosing appropriate functional forms which can be liable to data availability or applicability of certain functional forms in the region.

Here, we mention applicable forms for IPEs developed in past studies for the Himalayas and other world areas. For some IPEs, intensity attenuation with distance is defined in terms of epicentral intensity (I_0) based on the assumptions that the intensity is proportional to the logarithm of the energy density or its power and that the seismic source is a point source (Howell and Schultz 1975). Chandra 1980; Ghosh and Mahajan 2013 (Table 1) have used this functional form for their IPEs. Some IPEs are in terms of earthquake magnitude (first-order fit) and a distance metric such as epicentral (R_{epi}) or hypocentral (R_{hyp}) distance. Their functional form is given as

$$I = a + bM + c\ln R + dR \qquad (1)$$

Here, M is the magnitude for the earthquake event, R is the R_{epi} or R_{hyp}. "a" is a calibration or scaling parameter; "b" represents dependence on magnitude or energy released; "c" represents geometrical spreading which assumes a wavefront radiating from a point source and distributing over a spherical surface of

increasing size; "*d*" is anelastic or intrinsic attenuation (energy absorption due to internal friction) factor. Ambraseys and Douglas (2004), Szeliga et al. (2010), and Ghosh and Mahajan (2011) (Table 1) have used this functional form while using different magnitude scales for their IPEs.

For IPE development, certain authors (Musson 2005; Atkinson and Wald 2007; Atkinson et al. 2014) have given IPE functional form, as used by Boore et al. (1993) in GMPE developed from North American earthquakes. The functional form used by them has magnitude (a second-order fit) and distance terms which have a non-linear relation with the intensity (*I*) given as

$$I = c_1 + c_2(M-6) + c_3(M-6)^2 + c_4R + c_5\log_{10}R + c_6M\log_{10}R + c_7B \quad (2)$$

Here, c_1, c_2, c_3, c_4, c_5, c_6, and c_7 are regression coefficients, M is earthquake magnitude, R is epicentral distance, and $B = max\{0, \log_{10}(R/50)\}$. We have not used the epicentral intensity functional form in the present study because of the problems associated with the determination of epicentral intensity, I_0 (Ambraseys 2001; Musson 2005). For some earthquake events, the epicentral intensity value is less than the maximum intensity value observed. I_0-based equations do not capture this effect. We have used Eq. (2) but without the B term and using M instead of (M-6), as it has only a cosmetic effect on the final equation (Musson 2005).

In this study, we have developed separate IPEs for the data available from traditional sources and internet-based questionnaires for the Himalayas and its sub-regions. Then, the attenuation behaviour of the newly developed IPEs is compared with the previously available IPEs for the region. A likelihood-based method has been used to assess the performance of the IPEs for the events not considered in the IPE development.

2 Dataset

Intensity data of an earthquake is available in different forms whose quality depends upon the accuracy of the assigned intensity value's reported location and the observer's knowledge and experience. Allen et al. (2008) have defined a quality ranking (highest to lowest) for the data collected from different studies depending upon the method used, as follows:

1. Macroseismic intensities are assigned with latitude and longitude site locations, also known as Intensity Data Points (IDPs).
2. The historical or modern maps are digitized to assign intensity for different sites.
3. Did You Feel It? (or DYFI) data format by Atkinson and Wald (2007) uses a standard questionnaire.
4. Intensity values are assigned from isoseismal contours by digitizing isoseismal maps of earthquake events.

Types 1, 2, and 4 are generally categorized as traditional sources, whereas Type 3 is an internet-based questionnaire (Hough and Martin 2021). In the present study, we have used two datasets—one containing Intensities from traditional sources based on IDPs (hereafter referred to as the TRAD dataset) and another based on DYFI reports. The naming convention used for datasets (i.e., TRAD and DYFI) is the same as that used by Hough and Martin (2021). A list of all the events considered for the IPE development with their descriptions and macroseismic data sources is given in Table 2 and 3. Figure 1a shows the epicentral location and magnitude of the events considered for both datasets occurring between 1950 and 2021.

We have used past studies with reported intensities in the literature for the preparation of the TRAD dataset. For the earthquake events till 2009, we have used the intensity data from the catalogue prepared by Martin and Szeliga (2010). We have collected macroseismic data reported in the literature for the six events occurring between 2011 and 2020. Studies conducted by Prajapati et al. (2013), Martin et al. (2015), Gupta et al. (2013), Gahalaut et al. (2016), Debbarma et al. (2017), and Bharali et al. (2021) have been used for the traditional macroseismic data. Due to the availability of earthquake intensity data in different intensity scales, an equivalence is required between the scales to use the data. In the present study, we used the conversion relation given by Musson et al. (2010) between different scales and EMS-98 to use historical and current data available in other datasets under a single scale for analysis. We have adopted the following criteria for reassessment and inclusion of the reported intensities in our final TRAD dataset:

Table 2 Events considered for the traditional dataset (or TRAD), along with their parameters and references. Events' dates are as per Indian Standard Time (IST)

S. No	Earthquake		Epicentre		M_w	Depth (km)	I_{max}	IDPs	Scale	Reference
	Date	Designation	Lat (°N)	Long (°E)						
1	15 Aug 1950	ASSAM-1950	28.36[u]	96.44[u]	8.6[u]	15.0[u]	9	68	EMS-98	Martin and Szeliga (2010)
2	10 Oct 1956	KHURJA-1956	28.15	77.67	6.0[#]	15	7	18		
3	27 Aug 1960	GURGAON-1960	28.47[s]	77.00[s]	4.8[s]	15.0[s]	7	41		
4	19 Jan 1975	KINNAUR–1975	32.46[i]	78.43[i]	6.8[i]	7.5[i]	8	28		
5	29 Jul 1980	BAJHANG–1980	29.60[i]	81.09[i]	6.6[i]	15.0[i]	8	19		
6	26 Apr 1986	DHARAMSALA–1986	32.13[u]	76.37[u]	5.5[u]	33.0[u]	7	19		
7	06 Aug 1988	INDO-BURMA-1988	25.09[e]	95.11[e]	7.3[e]	90[e]	6	32		
8	20 Aug 1988	UDAYPUR–1988	26.76[u]	86.62[u]	6.9[u]	57.4[u]	8	190		
9	20 Oct 1991	UTTARKASHI–1991	30.78[i]	78.77[i]	6.8[i]	11.6[i]	9	107		
10	29 Mar 1999	CHAMOLI–1999	30.51[u]	79.4[u]	6.6[u]	15.0[u]	8	281		
11	26 Jul 2003	KOLABONIA-2003	22.90[g]	92.30[g]	5.6[g]	15.0[g]	7	17	EMS-98	Martin and Szeliga (2010)
12	08 Oct 2005	KASHMIR-2005-A	34.45[u]	73.65[u]	7.6[u]	26.0[u]	9	294		
13	14 Dec 2005	GHARWAL-2005-B	30.48[u]	79.26[u]	5.1[u]	44.0[u]	6	22		
14	14 Feb 2006	SIKKIM-2006	27.38[u]	88.36[u]	5.3[u]	30.0[u]	7	58		
15	05 Aug 2006	KUMAON-2006-B	29.89[u]	80.10[u]	4.6*	10.0[u]	6	19		
16	20 May 2007	SIKKIM-2007-B	27.23[g]	88.56[g]	4.9[g]	13.6[g]	5	20		
17	26 Nov 2007	DELHI-2007	28.56[u]	77.06[u]	4.7*	10[u]	5	54		
18	20 Feb 2009	KASHMIR-2009-A	34.20[u]	73.90[u]	5.5	12	7	35		
19	18 Sep 2011	SIKKIM-2011	27.72[r]	88.14[r]	6.9[r]	50[r]	9	674	MMI, EMS-98	Prajapati et al. (2013), Martin and Hough (2015)
20	5 Mar 2012	DELHI-2012	28.73[s]	76.60[s]	4.6[s]	15[s]	6	62	MMI	Gupta et al. (2013)
21	25 Apr 2015	NEPAL-2015	28.23[u]	84.73[u]	7.8[u]	8.2[u]	9	3159	EMS-98	Martin et al. (2015)
22	4 Jan 2016	MANIPUR-2016	24.80[u]	93.65[u]	6.7[u]	55[u]	7	394	EMS-98	Gahalaut et al. (2016)
23	3 Jan 2017	TRIPURA-2017	24.02	91.96	5.6	31	7	95	EMS-98	Debbarma et al. (2017)
24	22 Jun 2020	MIZORAM-2020	23.14[u]	93.29[u]	5.6[u]	10.8[u]	8	36	MMI	Bharali et al. (2021)

M_w moment magnitude, mb body-wave magnitude, I_{max} maximum intensity, IDP intensity data point

[#]From Gupta et al. (1998)

*M_w obtained after using Das et al. (2011) relationship between M_w and mb

[u]From USGS ANSS Comprehensive Earthquake Catalog (ComCat); [i]From ISC–GEM catalog (Storchak et al. 2013, 2015)

[r]From Rajendran et al. (2011)

[s]From Singh et al. (2013)

[e]From Engdahl and Villasenor (2002)

[g]From GCMT Catalog (http://www.globalcmt.org)

Table 3 List of earthquake events considered for the DYFI Dataset along with their parameters and references. Events' dates are as per Indian Standard Time (IST)

S. No	Event		Epicentre		M_w	Depth (km)	I_{max}	IDPs	Scale	ComCat EventID
	Date	Designation	Lat (°N)	Long (°E)						
1	04 Feb 2011	INDO-MYANMAR-2011	24.62	94.68	6.2	85	6	51	MMI	usp000hu2t
2	18 Sep 2011	SIKKIM-2011	27.72[r]	88.14[r]	6.9[r]	50[r]	8	198		usp000j88b
3	09 Feb 2012	UTTARAKHAND-2012	30.99	78	5.3	6.2	6	19		usp000jerg
4	5 Mar 2012	DELHI-2012	28.73[s]	76.60[s]	4.6[s]	15[s]	5	27		usp000jfth
5	11 May 2012	ASSAM-2012	26.18	92.89	5.4	43.3	6	28		usp000jka9
6	01 May 2013	JAMMU-2013	33.06	75.86	5.7	15.0	5	34		usb000gjhz
7	25 Apr 2015	NEPAL-2015	28.23	84.73	7.8	8.2	8	327		us20002926
8	4 Jan 2016	MANIPUR-2016	24.80	93.65	6.7	55	8	164		us10004b2n
9	27 Nov 2016	NEPAL-2016	27.80	86.53	5.2[i]	10.0	5	31		us10007cuh
10	3 Jan 2017	TRIPURA-2017	24.02	92.02	5.7	32	6	40	MMI	us10007pfk
11	06 Feb 2017	UTTARAKHAND-2017	30.65	79.16	5.1	16.1	5	92		us20008hyg
12	12 Sep 2018	ASSAM-2018	26.37	90.16	5.3	10.0	6	54		us2000hd8v
13	24 Apr 2019	ARUNACHAL-2019A	28.41	94.56	5.9	14.0	7	49		us70003axc
14	19 Jul 2019	ARUNACHAL-2019B	27.72	92.83	5.5	15.0	5	29		us70004nrn
15	22 Jun 2020	MIZORAM-2020	23.14	93.29	5.6	10.8	4	7		us6000ag4u
16	05 Apr 2021	SIKKIM-2021	27.19	88.94	5.4	10.0	6	63		us6000dz5d
17	28 Apr 2021	ASSAM-2021	26.78	92.46	6.0	34.0	9	78		us7000dy3b
18	07 Jul 2021	MEGHALAYA-2021	25.96	90.35	5.3	10.0	7	26		us7000ej9c

ComCat EventID given in the table will be used as "EVENTID" at the following web address: http://earthquake.usgs.gov/earthquakes/eventpage/EVENTID

M_w moment magnitude, I_{max} maximum intensity, *IDP* Intensity Data Point

[u]From USGS ANSS Comprehensive Earthquake Catalog (ComCat)

[r]From Rajendran et al. (2011)

[i]From ISC-GEM catalog (Storchak et al. 2013, 2015)

[s]From Singh et al. (2013)

[e]From Engdahl and Villasenor (2002)

[g]From GCMT Catalog (http://www.globalcmt.org)

1. Only intensities with exact locations and with numeral assignment values are included.
2. Due to the non-availability of descriptive information for re-assignment and use of the term *"Felt…"* being used for a range of Intensities on the EMS-98 scale (see description for EMS Intensity II, III, IV, and V in Grünthal et al. 1998), we have discarded the IDPs with assignment "F".
3. The "round half up" rule was used for reassigning fractional Intensity values to be more conservative. Intensity values were assumed to be reported in fractions for a particular intensity assignment because a substantial number of observations corresponds to an Intensity value greater than the nearest lowest integer intensity value. This rule is like what Sørensen et al. (2009) used for developing IPEs for a sub-region of Northwest Turkey. Musson (2005) advocated an opposite scheme to get Intensity values using their IPEs developed for the UK. Their data was from isoseismal maps (which have a different meaning than IDPs), which also changed the interpretation of the IPEs developed for the UK.
4. Intensities describing geotechnical effects like landslides, ground spreading and liquefaction were not considered.

Fig. 1 Himalayan earthquake event epicentre locations with their respective occurrence year from TRAD (in bold) and DYFI (in italics) datasets, along with some of its tectonic features highlighted. **b** Sub-regions of Himalaya (with Central Himalaya highlighted by yellow background) used for separate Intensity Prediction Equation (IPE) development along with their Intensity Data Points (IDPs) from both traditional (TRAD) and online (DYFI) datasets. Earthquakes' moment magnitude (M_w) has also been shown for all the events. KFL—Karakoram Fault Line, ITS—Indo-Tsangpo Suture, IEPB—Indo-Eurasian plate Boundary, SF—Sagaing Fault, DT—Dauki Thrust

(a)

(b)
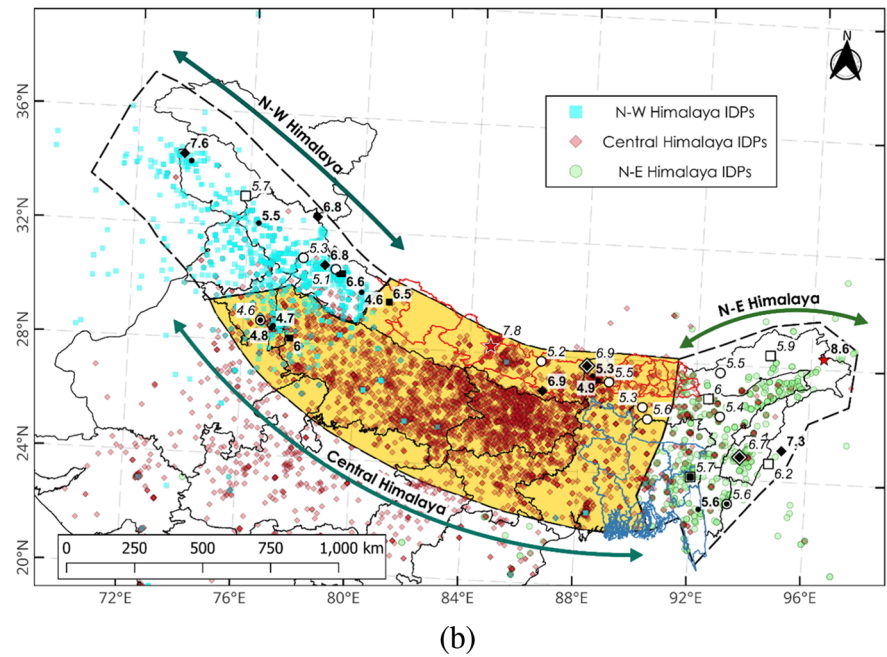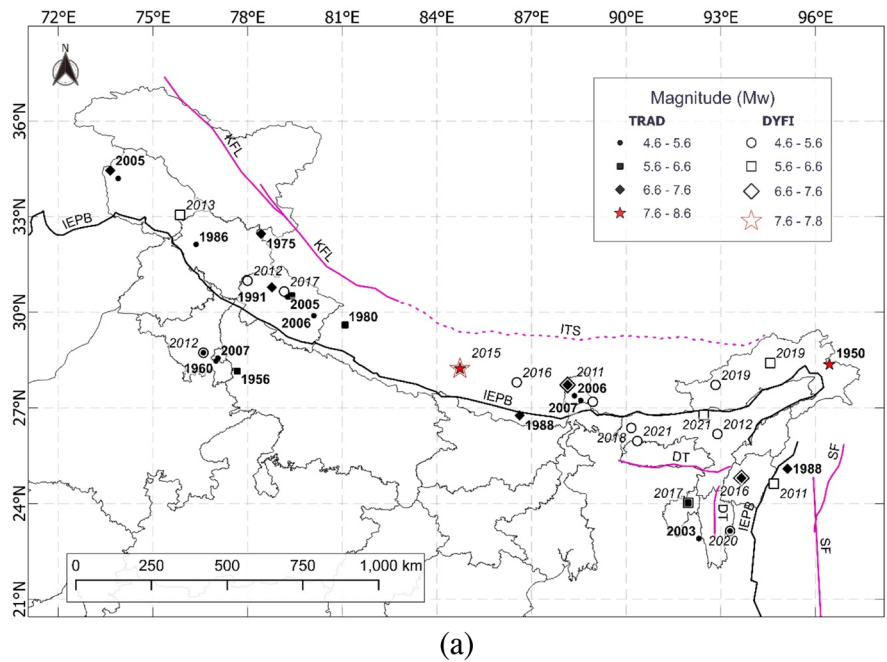
5. We have considered only those earthquake events from Martin and Szeliga's (2010) dataset that occurred after 1950 in the Himalayas and have more than 15 IDPs reported.

6. Due to a lack of information about building types for some VIII + Intensity reports Prajapati et al. (2013), we adopted the following criteria for the Intensity assignment—for locations where *many* buildings were damaged, or a *few* were destroyed, we have assigned Intensity IX. For sites where reports did not explicitly mention the damage to the infrastructure, we have given an intensity value of VIII (from VIII +).
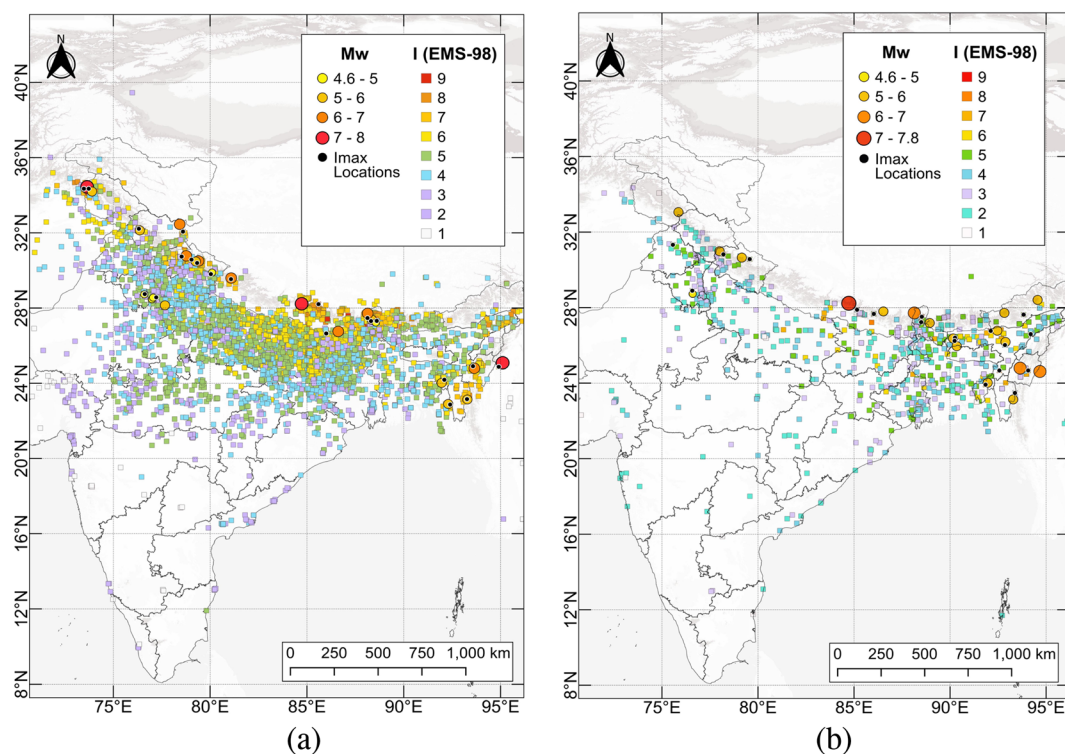
Fig. 2 **a** TRAD (or traditional) and **b** DYFI (Did You Feel IT?) intensities for Himalayan Earthquakes along with their epicentral locations and magnitudes. Maximum intensity and I_{max} locations are also indicated (with black dots) for both datasets

Our final datasets have 5742 and 1317 IDPs for TRAD and DYFI, respectively. Figure 2a, b shows the location of these IDPs. Compared to TRAD, the DYFI IDPs are sparse and reported more in the North-East Himalayas than in the Northwest Himalayas, as many events in the DYFI are mainly in the former region for the considered period. The maximum intensity reported in both datasets is IX on the EMS-98 scale. Figure 3 shows observed I and M_w variation for R_{hyp} for both datasets. For TRAD and DYFI datasets, 72.5% and 91.8% of IDPs are below Intensity VI (EMS-98), respectively (Fig. 3e, f), which indicates that the TRAD intensities may be better suitable for predicting Intensities at higher levels as more accounts are available for these values.

To compare predicted intensities from TRAD and DYFI datasets, we have considered six earthquake events—SIKKIM-2011, DELHI-2012, NEPAL-2015, MANIPUR-2016, TRIPURA-2017, and MIZO-RAM-2020, for which data is available in both TRAD and DYFI datasets. Complete TRAD and DYFI datasets were also considered for regression analysis to get IPEs for the Himalayan region. As we have many earthquake events, we

have divided the Himalayan region into three zones. Along the lines of Chandra (1980), these divisions are North-West (N-W) Himalaya, Central Himalaya (instead of Ganga basin), and North-East (N-E) Himalaya (Table 4).

Intensity is a function of source, source-to-site distance, site condition and building types, and these parameters vary across regions. So, for intensity prediction, it will be suitable to develop region-specific equations. We have done this division to segregate different regions' source and site effects in the IPEs (Fig. 1b). Also, it helps in differentiating Intensity attenuation characteristics at global (or macro) and regional (micro) levels. This segregation has been done while considering the tectonics, site characteristics and building types of the locations where different events have occurred. Our classification is similar to Rajendran et al. (2017) who have classified the Himalayan arc similarly based on its seismotectonics. As site characteristics influence the attenuation characteristics of earthquake waves near the surface, e.g. rocky hills and alluvium plains may amplify or attenuate the earthquake's effects (Geli et al. 1988;

Fig. 3 Intensity-distance variation in **a** and **b**, magnitude-distance distribution in **c** and **d**, and intensity-frequency in **e** and **f**, for TRAD and DYFI datasets, respectively
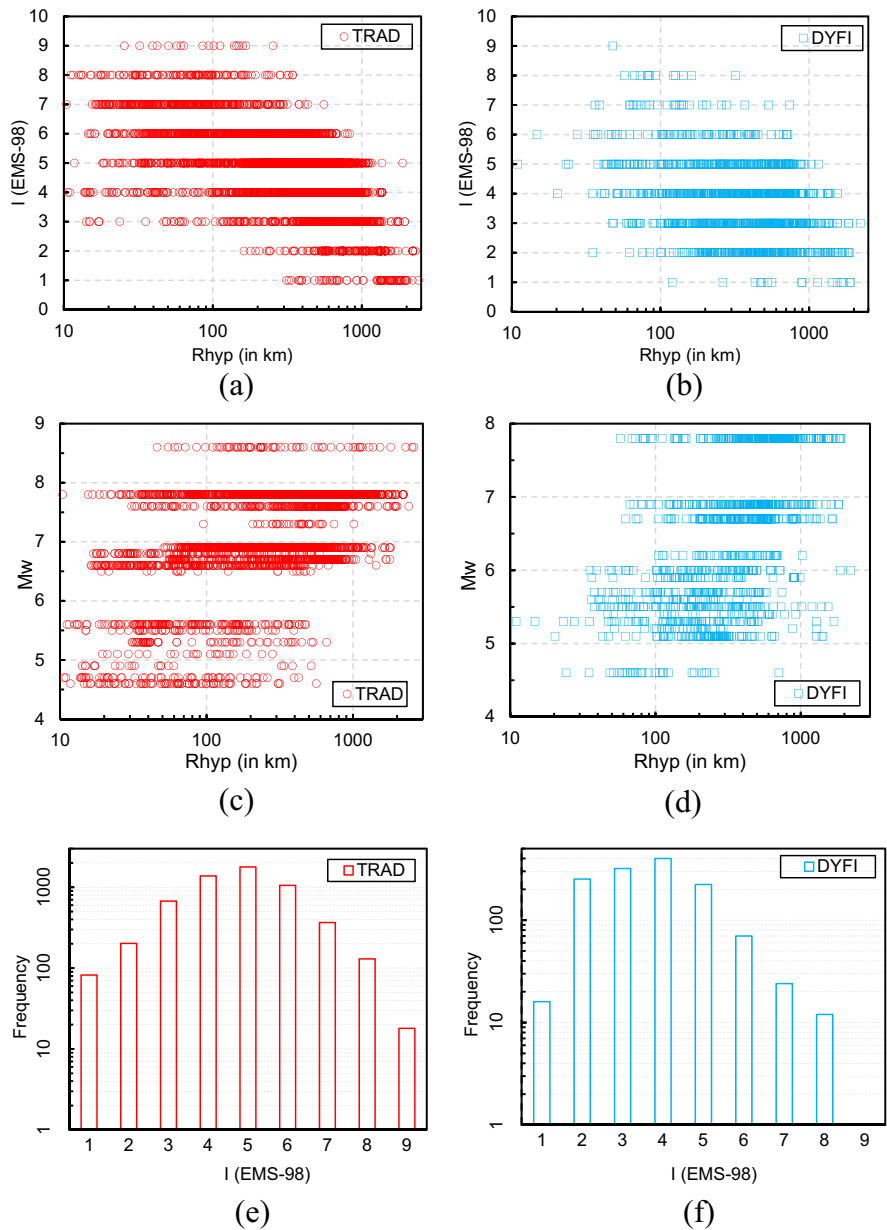
Pitilakis 2004; Kaiser et al. 2013), dividing regions for IPEs applicability seems suitable. Also, Intensity values assigned to an area after an earthquake depend upon the building stock types of that area (Grünthal et al. 1998; Dolce et al. 2003; Goda et al. 2015). In the Himalayan region, building stock types vary across different states (BMTPC 2019). Building types' numbers and percentages in the N-W Himalayas differ from those in the N-E Himalayas and Central Himalayan states (BMTPC 2019).

N-W Himalayan events in our dataset lie along the Panjal Thrust, which includes Hazara-Kashmir syntaxis (Yeats 2012). For the N-E Himalayan events, we have considered those events whose focus lies closer to or along the Sagaing fault along the transform boundary formed by the Indian and Sunda plates (Fig. 1a, b).

Table 4 List of events used for IPE development for the sub-region of Himalaya. The events listed here are taken from TRAD and DYFI datasets in Table 2 and 3, respectively

TRAD events				DYFI events			
S. No	Event	M_w	IDPs	S. No	Event	M_w	IDPs
North-West Himalaya							
1	KINNAUR-1975	6.8	28	1	UTTARAKHAND-2012	5.3	19
2	DHARAMSALA-1986	5.5	19	2	JAMMU-2013	5.7	34
3	UTTARAKASHI-1991	6.8	107	3	UTTARAKHAND-2017	5.1	92
4	CHAMOLI-1999	6.6	281				
5	KASHMIR-2005-A	7.6	294				
6	GHARWAL-2005-B	5.1	22				
7	KUMAON-2006-B	4.6	19				
8	KASHMIR-2009-A	5.5	35				
Central Himalaya							
1	KHURJA-1956	6.0	18	1	SIKKIM-2011	6.9	198
2	GURGAON-1960	4.8	41	2	DELHI-2012	4.6	27
3	BAJHANG-1980	6.6	19	3	NEPAL-2015	7.8	327
4	UDAYPUR-1988	6.9	190	4	NEPAL-2016	5.2	31
5	SIKKIM-2006	5.3	58	5	ASSAM-2018	5.3	54
6	SIKKIM-2007-B	4.9	20	6	SIKKIM-2021	5.5	63
7	DELHI-2007	4.7	54	7	MEGHALAYA-2021	5.6	26
8	SIKKIM-2011	6.9	674				
9	DELHI-2012	4.6	62				
10	NEPAL-2015	7.8	3159				
North-East Himalaya							
1	ASSAM-1950	8.6	68	1	INDO-MYANMAR-2011	6.2	51
2	INDO-BURMA-1988	7.3	32	2	ASSAM-2012	5.4	28
3	KOLABONIA-2003	5.6	17	3	MANIPUR-2016	6.7	164
4	MANIPUR-2016	6.7	394	4	TRIPURA-2017	5.7	40
5	TRIPURA-2017	5.6	95	5	ARUNACHAL-2019A	5.9	49
6	MIZORAM-2020	5.6	36	6	ARUNACHAL-2019B	5.5	29
				7	MIZORAM-2020	5.6	7
				8	ASSAM-2021	6.0	78

Hence, the events occurring in Sikkim-Himalaya have been considered part of the Central Himalaya dataset. In the future, the Central Himalayan region in our dataset can be further divided into the "Ganga Basin" and "Sikkim Himalaya" sub-regions as data from more significant events become available.

3 Methodology

3.1 Regression analysis

For developing IPEs from the datasets considered in the present study, we have used the two-stage regression analysis method by Joyner and Boore (1981) (hereafter referred to as TSRA) and a multiple regression analysis (MRA) procedure. TSRA has been used for GMPE development as it decouples the magnitude dependence of the dependent variable from the distance dependence. For the first stage of TSRA, we have used the functional form given:

$$I = \sum_{i=1}^{N} \alpha_i E_i + dR_{hyp} + e \ln\left(R_{hyp}\right) \quad (3a)$$

where $E_i = 1$ for earthquake I.

   $= 0$ otherwise.

   $R_{hyp} =$ hypocentral distance.

$$= \sqrt{\left(R_{epi}^2 + h^2 \right)}; \text{ here } R_{epi} = \text{Epicentral distance},$$

$h =$ focal depth.

$I =$ macroseismic intensity (EMS-98).

In the first stage, coefficients α_i, d, and e are obtained by linear regression analysis. In the second stage, α_i are used to find the coefficient corresponding to the magnitude for a first or second-order dependence using the following relation:

$$\alpha_i = a + bM_i + cM_i^2 \tag{3b}$$

where $M_i =$ magnitude of earthquake i. For getting a linear (first-order) relation w.r.t magnitude $c = 0$. The final functional form is given as

$$I = a + bM + cM^2 + dR_{hyp} + e\ln\left(R_{hyp}\right) \tag{4}$$

Here we used moment magnitude (M_w) and also new generalized moment magnitude scale (M_{wg}) also known as Das magnitude scale developed by Das et al. (2019). M_{wg} applies to a wide earthquake magnitude range and represents better for seismic moment for moment magnitudes less than 7.5 (Das et al. 2023). In the present study, we have regressed the data w.r.t M_w for IPEs, but given the applicability range of IPEs in both M_w and M_{wg} scales for robust predictions w.r.t earthquake magnitude. Further, we have utilized relationships between magnitude scales and seismic moment (M_0) given by Das et al. (2019) (for M_{wg} vs. M_0) and Hanks and Kanamori (1979) (for M_w and M_0) to arrive relation between M_w and M_{wg}.

$$M_w = \frac{2}{3}\log M_0 - 10.7 \tag{5a}$$

Substituting seismic moment, M_0 into Das et al. (2019) relation, which is given as

$$M_{wg} = \frac{\log M_0}{1.36} - 12.68 \tag{5b}$$

The final relationship between M_w and M_{wg} obtained is given as

$$M_{wg} = 1.103 M_w - 0.878 \tag{5c}$$

This relation has been used to calculate the magnitude applicability range of IPEs. The above relationship also confirms the observations made by Das et al. (2019) and Das et al. (2023) that in magnitudes less than 7.5, the M_w scale overestimates the earthquake magnitudes while closely matching for the higher values ($7.5 \leq$ magnitude ≤ 9.0) with M_{wg}. Figure 4a shows the relation between M_w versus M_{wg} given by Eq. (5c); also, data points of Table 3 are from Das et al. (2019).

3.2 IPE comparison for prediction

Log-likelihood or LLH method (Scherbaum et al. 2009; Delavaud et al. 2012) has been used to assess IPE performance for events (other than those considered in the dataset) that occurred in the Himalayan region. This method has been used in past studies for testing the performance and ranking of GMPEs in seismic hazard studies (Beauval et al 2012; Anbazhagan et al. 2016; Bajaj and Anbazhagan 2019; Alpyürür and Lav 2022). LLH is defined as

$$\text{LLH}(g, y) = -\frac{1}{n} \sum_{i=1}^{N} \log_2\left(g\left(y_i\right)\right) \tag{6}$$

Here, $y = \{y_i\}$, $i = 1, \ldots, N$ are the observation from the event for which IPE performance is being compared at an epicentral/hypocentral distance R_j, and $g(y_i)$ is the probability density function (Fig. 4b). LLH value for each event is calculated using mean values predicted through respective IPEs and their standard deviation (σ) values assuming a normal distribution.

Here,

$$g\left(y_i\right) = \frac{1}{\sigma\sqrt{2\pi}}\exp\left(\frac{y_i - I_{pred,j}}{\sigma}\right)^2 \tag{7}$$

Here, $I_{pred,j}$ is the predicted intensity value by an IPE at the distance R_j. LLH methods measure the likelihood that the considered model has produced the dataset for a particular event.

4 Results and discussion

Coefficients obtained after TSRA for different datasets are given in Table 5. Next, we performed MRA on all the datasets' results, which are given in Table 6.

Fig. 4 **a** Generalized moment magnitude (M_{wg}) vs. moment magnitude (Mw) relationship shown using Eq. 5(c). Calculated M_w and M_{wg} values given in Das et al. (2019) Table 3 (394) events are also shown. **b** Schematics of LLH method applied to a typical earthquake IDPs

(a)

(b)
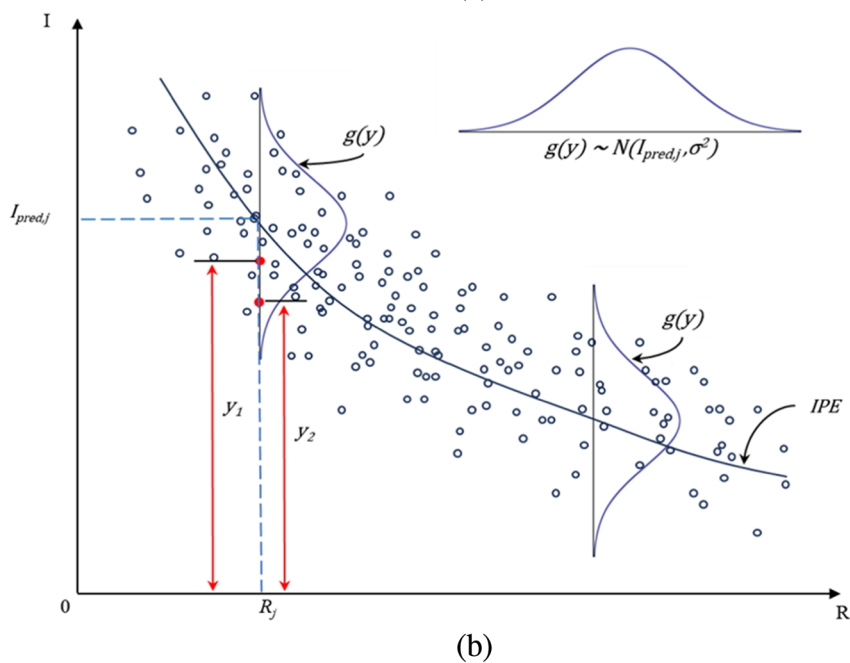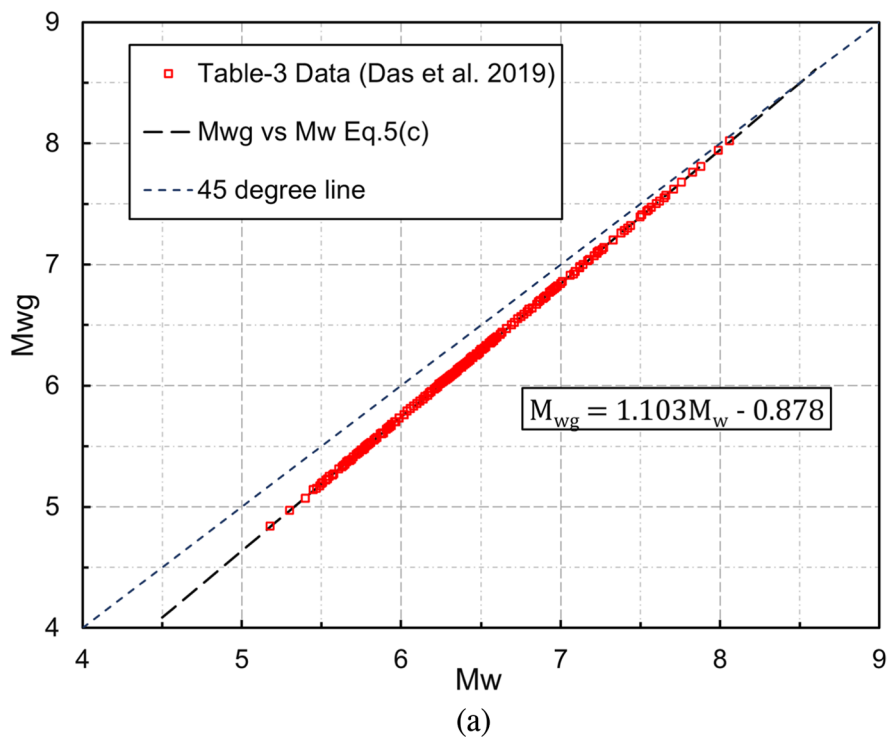
4.1 IPEs for events with both TRAD and DYFI data

To compare the intensity attenuation behaviour for data collected using traditional sources and Internet-based questionnaires, data from the six earthquake events' TSRA IPEs is considered. Figure 5 shows the I (EMS-98) plot vs. R_{epi} for an earthquake of M_w 7.0 and M_w 5.0. Coefficients obtained by TSRA (Table 5) are used for

Table 5 Coefficients value for IPEs (with first-order and second-order relation w.r.t. M_w) of functional form $I = a + b\,M_w + c\,M_w^2 + d\,R_{hyp} + e\,\ln(R_{hyp})$ using TSRA. "Six TRAD (/DYFI) events" refer to the events with Intensity data available in both TRAD and DYFI datasets, i.e., SIKKIM-2011, DELHI-2012, NEPAL-2015, MANIPUR-2016, TRIPURA-2017, and MIZORAM-2020

Two-stage regression analysis (TSRA) results

Dataset	a	b	c	d	e	Adjusted R-square	RMSE (σ)
Six TRAD events	6.15	0.55	–	−0.0012	−0.84	0.51	0.91
Six DYFI events	4.70	0.91	–	−0.00007	−1.20	0.26	1.20
TRAD dataset	3.50	0.96	–	−0.0011	−0.92	0.54	0.94
DYFI dataset	4.31	0.84	–	−0.00003	−1.04	0.29	1.11
N-W Himalaya TRAD	2.76	1.16	–	−0.0013	−1.05	0.75	0.78
Central Himalaya TRAD	2.33	1.08	–	−0.0013	−0.84	0.45	0.99
N-E Himalaya TRAD	6.89	0.38	–	−0.0012	−0.77	0.57	0.92
N-W Himalaya DYFI	1.30	0.8	–	−0.0006	−0.45	0.08	0.93
Central Himalaya DYFI	4.58	0.81	–	−0.00017	−1.06	0.32	1.13
N-E Himalaya DYFI	5.27	0.93	–	0.00079	−1.33	0.31	1.08
Six TRAD events	0.008	2.59	−0.16	−0.0012	−0.84	0.52	0.90
Six DYFI events	4.71	0.90	0.0002	−0.00007	−1.20	0.26	1.20
TRAD dataset	−2.34	2.86	−0.15	−0.0011	−0.92	0.56	0.91
DYFI dataset	0.14	2.22	−0.11	−0.00003	−1.04	0.31	1.10
N-W Himalaya TRAD	5.93	0.09	0.09	−0.0013	−1.05	0.75	0.78
Central Himalaya TRAD	0.70	1.63	−0.05	−0.0013	−0.84	0.47	0.96
N-E Himalaya TRAD	16.84	−2.56	0.21	−0.0012	−0.77	0.53	0.95
N-W Himalaya DYFI	233.76	−85.24	7.95	−0.0006	−0.45	0.15	0.89
Central Himalaya DYFI	3.20	1.27	−0.04	−0.00017	−1.06	0.32	1.12
N-E Himalaya DYFI	−6.96	5.00	−0.34	0.00079	−1.33	0.31	1.08

these attenuation curves. From Fig. 5, one can observe that TRAD-based IPEs consistently predict higher Intensities than DYFI. Predicted intensities using TRAD are higher by almost half to one complete Intensity unit between 50 and 700 km for M_w 7.0. The difference in predicted intensity is more pronounced for an M_w 5.0 earthquake, where predicted intensity using DYFI is a unit lower than TRAD-based prediction. The influence of attenuation due to geometric spreading is more significant in the DYFI than in the TRAD dataset. The anelastic attenuation effect is negligible for the DYFI over the whole distance range (Fig. 5).

In comparison, its influence can be seen in TRAD IPEs after an approximate distance of 200 km for all three M_w, where the rate of intensity attenuation increases. The discrepancy in the effect of anelastic attenuation in the TRAD and DYFI datasets may pertain to the difference in their characteristics, or one may represent the region's attenuation behaviour. This remains inconclusive as the number of earthquakes is significantly less, and the area under observation is large. As the magnitude value increases, this difference reduces for both the first and second order fit (Fig. 5).

4.2 Comparison of two-stage (TSRA) and one-stage regression (MRA)

Musson (2005) has discussed using two-stage or one-stage regression procedures for IPEs while questioning the advantage of TSRA against a one-stage regression procedure (such as MRA). As in IPEs, intensity (the dependent variable) is not derived using instrumental data, and M_w (the independent variable) is derived using instrumental data; the error in measuring M_w will not affect the errors in distance coefficients. However, this is not the case with GMPEs, where dependent variables such as Peak Ground Acceleration (PGA) or Peak Ground Velocity (PGV) are also obtained from instrumental data. To check the adequacy of TSRA for our datasets, we have used MRA w.r.t. M_w and R_{hyp} for the functional form given by Eq. (5). The obtained MRA and TSRA results (Table 5 and 6) are comparable from the point of view of R-square and RMSE (or standard deviation, σ in this case). MRA's R-square values are equal to or slightly greater than corresponding TSRA values for all

Table 6 Coefficients value for IPE of functional form $I = a + b\,M_w + c\,M_w^2 + d\,R_{hyp} + e\,ln\,(R_{hyp})$ using MRA. "Six TRAD (/DYFI) events" refer to the events with intensity data available in both TRAD and DYFI datasets, i.e., SIK-KIM-2011, DELHI-2012, NEPAL-2015, MANIPUR-2016, TRIPURA-2017, and MIZORAM-2020

Multiple regression analysis (MRA) results

Dataset	a	b	c	d	e	Adjusted R-square	RMSE (σ)
Six TRAD events	6.54	0.46	–	− 0.0012	− 0.80	0.52	0.90
Six DYFI events	5.16	0.70	–	− 0.0004	− 1.00	0.28	1.19
TRAD dataset	4.80	0.70	–	− 0.0013	− 0.81	0.55	0.92
DYFI dataset	4.66	0.69	–	− 0.00028	− 0.91	0.30	1.1
N-W Himalaya TRAD	2.65	1.18	–	− 0.0013	− 1.05	0.75	0.78
Central Himalaya TRAD	4.31	0.68	–	− 0.0016	− 0.69	0.51	0.93
N-E Himalaya TRAD	6.27	0.54	–	− 0.00089	− 0.87	0.58	0.91
N-W Himalaya DYFI	1.79	0.55	–	− 0.00092	− 0.24	0.12	0.92
Central Himalaya DYFI	4.58	0.74	–	− 0.00037	− 0.96	0.32	1.13
N-E Himalaya DYFI	6.73	0.67	–	0.00076	− 1.30	0.31	1.08
Six TRAD events	0.43	2.37	− 0.14	− 0.0011	− 0.86	0.52	0.9
Six DYFI events	− 1.38	2.93	− 0.17	− 0.00012	− 1.16	0.28	1.18
TRAD dataset	− 4.01	3.46	− 0.20	− 0.0012	− 0.87	0.57	0.91
DYFI dataset	− 2.92	3.18	− 0.19	− 0.00011	− 0.98	0.32	1.09
N-W Himalaya TRAD	2.46	1.24	− 0.005	− 0.0013	− 1.05	0.75	0.78
Central Himalaya TRAD	− 5.21	3.80	− 0.24	− 0.0014	− 0.79	0.53	0.91
N-E Himalaya TRAD	3.58	1.37	− 0.06	− 0.0008	− 0.92	0.58	0.91
N-W Himalaya DYFI	233.76	− 85.24	7.95	− 0.00062	− 0.45	0.15	0.91
Central Himalaya DYFI	− 3.86	3.56	− 0.22	− 0.00017	− 1.06	0.34	1.11
N-E Himalaya DYFI	− 19.27	9.14	− 0.69	0.00074	− 1.27	0.32	1.08

datasets. Also, MRA's RMSE (here σ) values are equal to or less than values obtained from TSRA results, although the difference is negligible.

Next, the question comes as to which regression coefficients must be used for IPEs, as the adjusted R-square and RMSE values are almost similar for the two regression methods. It can be reasoned as follows: The IPE equation for its limiting case of a given minimum hypocentral distance should converge to the relation between I_{max} vs. M_w developed for the dataset, which has also been used for the equation. It implies that IPE should approximate an I_{max} vs. M_w relation at a *minimum hypocentral distance*. The determination of this hypocentral distance can be done as follows. In literature, IPEs have been derived using the following functional form (Eq. (1) + second-order term for M_w):

$$I = a + bM_w + cM_w^2 + d\sqrt{(R_{epi}^2 + h^2)} + e\ln\left(\sqrt{(R_{epi}^2 + h^2)}\right) \tag{8}$$

$$I = a + bM_w + cM_w^2 + dR_{hyp} + e\ln(R_{hyp}) \tag{9}$$

where R_{epi} refers to epicentral distance, h is the focal depth. The "h" in Eq. (8) is called nominal depth, h_0 (Musson 2005), and is derived (if not known) using MRA while optimizing the residuals. This h_0 can be used for our comparison of TSRA and MRA. But in the present case, we have derived IPEs as per Eq. (9) (as we have focal depth data available), and so we need a value of R_{hyp} at which we will check which one of our IPE (TSRA or MRA) better approximates the I_{max} vs. M_w relation.

For this, we minimized RMSE (Root-Mean Squared Error) for different values of R_{hyp} using Eq. (9) (with I_{max} and M_w from TRAD and DYFI) and obtained a value for which RMSE is the least. This R_{hyp} value we named "optimal depth", h_d. This h_d value is different from than h_0 value. Table 7 has RMSE results obtained based on h_d values, and the h_0 values are also reported. In Fig. 6, we plotted RMSE results from the RMSE minimization. The

Fig. 5 Variation of predicted intensity (I) w.r.t. epicentral distance (R_{epi}) for hypothetical M_w 7.0 (in **a, b**) and M_w 5.0 (in **c, d**) earthquakes using the six-earthquake data which have data available in both TRAD and DYFI datasets. IPE coefficients obtained from TSRA for "Six Trad Events" have been used (Table 5). In **e** and **f**, I_{max} w.r.t. M_w variation using the same IPEs has been shown
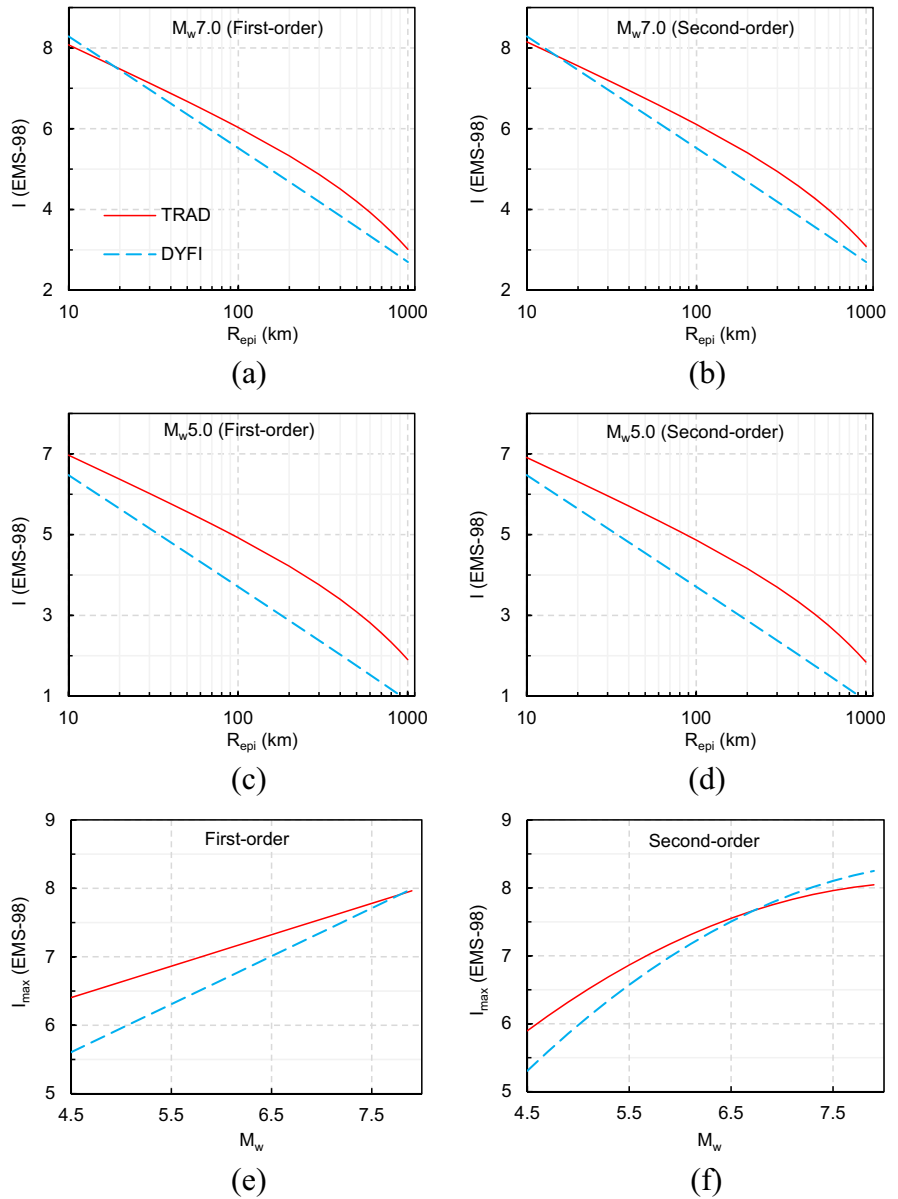
h_0 values were obtained for our TRAD and DYFI datasets following the procedure described by Musson 2005. The way h_d has been defined, its RMSE is supposed to be less than the RMSE obtained based on h_0 for the second-order TSRA and MRA IPEs derived based on R_{hyp}. So, we have used h_d's RMSE results to select TRAD and DYFI coefficients. Based on this, TRAD's MRA-based RMSE (0.74) and DYFI's TSRA-based RMSE (0.98) are the lowest (Table 7); hence, we would recommend the corresponding coefficients for IPEs.

We have used the same procedure for selecting the IPEs from TSRA and MRA for sub-regions of Himalaya. Based on RMSE results, one can argue that the difference in RMSE values obtained after applying IPEs approximation with I_{max} vs. M_w relation for the TSRA and MRA are insignificant. However, this comparison has been made to show how one can compare different IPEs for a region while giving more weightage to the I_{max} prediction capability of the IPEs. This procedure can also be used to get the h_d value for an IPE.

Table 7 Nominal (h_0) and optimal (h_d) depth results obtained for different IPEs (see text for explanation). Results of the minimum value of Root–Mean Squared Error (RMSE) corresponding to the h_d obtained from the I_{max} data for different regions and their respective predictive values are also given

Dataset (regression method)	h_0	h_d	RMSE (h_d)
TRAD (TSRA)	30	10	0.75
TRAD (MRA)	34	13	0.74
DYFI (TSRA)	19	9	0.98
DYFI (MRA)	17	16	0.99
N-W Himalaya TRAD (TSRA)	20	7	0.34
N-W Himalaya TRAD (MRA)	21	7	0.37
N-W Himalaya DYFI (TSRA)	7	22	0.57
N-W Himalaya DYFI (MRA)	7	28	0.58
Central Himalaya TRAD (TSRA)	59	9	0.58
Central Himalaya TRAD (MRA)	71	9	0.61
Central Himalaya DYFI (TSRA)	20	11	0.50
Central Himalaya DYFI (MRA)	19	13	0.51
N-E Himalaya TRAD (TSRA)	9	14	1.12
N-E Himalaya TRAD (MRA)	1	13	1.09
N-E Himalaya DYFI (TSRA)	23	13	1.30
N-E Himalaya DYFI (MRA)	21	16	1.30

4.3 IPE for the Himalayan region

Based on the beforementioned discussion, IPEs obtained from the MRA and TSRA for TRAD and DYFI datasets, respectively, for the whole Himalayan region are

$$I(\text{TRAD}) = -4.01 + 3.46M - 0.21M^2 - 0.0012R_{hyp} - 0.87\ln(R_{hyp})$$
$$\text{here } M \in \begin{cases} 4.6 \leq M_w \leq 8.6 \text{ if } M = M_w \\ 4.2 \leq M_{wg} \leq 8.6 \text{ if } M = M_{wg} \end{cases}$$
$$R^2 = 0.56, \sigma = 0.91; h_d = 13\text{km} \tag{10}$$

$$I(\text{DYFI}) = 0.14 + 2.22M - 0.11M^2 - 0.00003R_{hyp} - 1.04\ln(R_{hyp})$$
$$\text{here } M \in \begin{cases} 4.6 \leq M_w \leq 7.8 \text{ if } M = M_w \\ 4.2 \leq M_{wg} \leq 7.7 \text{ if } M = M_{wg} \end{cases}$$
$$R^2 = 0.31, \sigma = 1.10; h_d = 9\text{km} \tag{11}$$

Optimal depth (h_d) values are also given, which can be used as a minimum value of R_{hyp}. IPE's applicable magnitude (M_w or M_{wg}) range corresponds to the degree of magnitudes used for regression. Residual plots for Eqs. (10) and (11), indicating variation of residuals (ε) defined as (observed intensity, I_{obs})–(predicted intensity, I_{pred}) vs. R_{hyp} are shown in Fig. 7a, b, respectively. Also, median

residual values (lying closer to the zero axis), along with error bars representing a unit standard deviation, are shown in the figures. The slope and intercept term of a fit for residuals indicates that the mean error values are very close to zero over the R_{hyp} range.

4.4 IPE for North-West (N-W) Himalaya

For N-W Himalaya, IPEs are taken from the TSRA results for both TRAD and DYFI datasets, as the obtained RMSE (h_d) were the least for the TSRA. These IPEs are

$$I(\text{TRAD}) = 5.93 + 0.085M + 0.09M^2 + 0.0013R_{hyp} - 1.05\ln(R_{hyp})$$
$$\text{here } M \in \begin{cases} 4.6 \leq M_w \leq 7.6 \text{ if } M = M_w \\ 4.2 \leq M_{wg} \leq 7.5 \text{ if } M = M_{wg} \end{cases},$$
$$R^2 = 0.75, \sigma = 0.78; h_d = 7\text{km} \tag{12}$$

$$I(\text{DYFI}) = 233.76 - 85.24M + 7.95M^2 - 0.0006R_{hyp} - 0.45\ln(R_{hyp})$$
$$\text{here } M \in \begin{cases} 5.1 \leq M_w \leq 5.7 \text{ if } M = M_w \\ 4.7 \leq M_{wg} \leq 5.4 \text{ if } M = M_{wg} \end{cases},$$
$$R^2 = 0.15, \sigma = 0.89; h_d = 22\text{km} \tag{13}$$

The R-square value of 0.75 for Eq. (12) is the highest compared to all other IPEs, indicating that derived IPEs have relatively better prediction capability. In contrast, the same area's R-square value for DYFI data is the lowest. The low R-square value is because there are fewer events (only 3), and the observed scatter is more for a small magnitude range. A plot of residuals for Eqs. (12) and (13) is shown in Fig. 7c, d, respectively. The scatter of residuals shows that mean error values for TRAD-based IPEs are consistently closer to zero than their DYFI counterpart. This difference is primarily due to the low number of IDPs used for the N-W DYFI dataset (Table 4). For DYFI, the effect of fewer IDPs leading to non-zero mean residuals is more pronounced at near-site distances (<50 km).

Ghosh and Mahajan (2011), (2013) have given IPEs (G&M11 and G&M13 in Table 1) for N-W Himalaya based on the surface magnitude (M_s) scale. Das et al. (2011) relationship between M_s and M_w has been used (while using different formulas for conversion depending on magnitude range) to compare their IPEs with Eqs. (10) and (11). Intensity attenuation due to geometric spreading in Fig. 8 is almost similar for G&M11 and TRAD's IPE (Eq. (12)). Still, the predicted

Fig. 6 RMSE (Root-Mean Squared Errors) vs. R_{hyp} plots for TRAD in **a** and DYFI in **b** using Eq. (9). Coefficients used in Eq. (9) correspond to results obtained for second-order fit in Table 3 and 4. R_{hyp} values corresponding to minimum RMSE are "optimal depth, h_d" for that dataset, given in Table 7

(a)

(b)

(c)

(d)
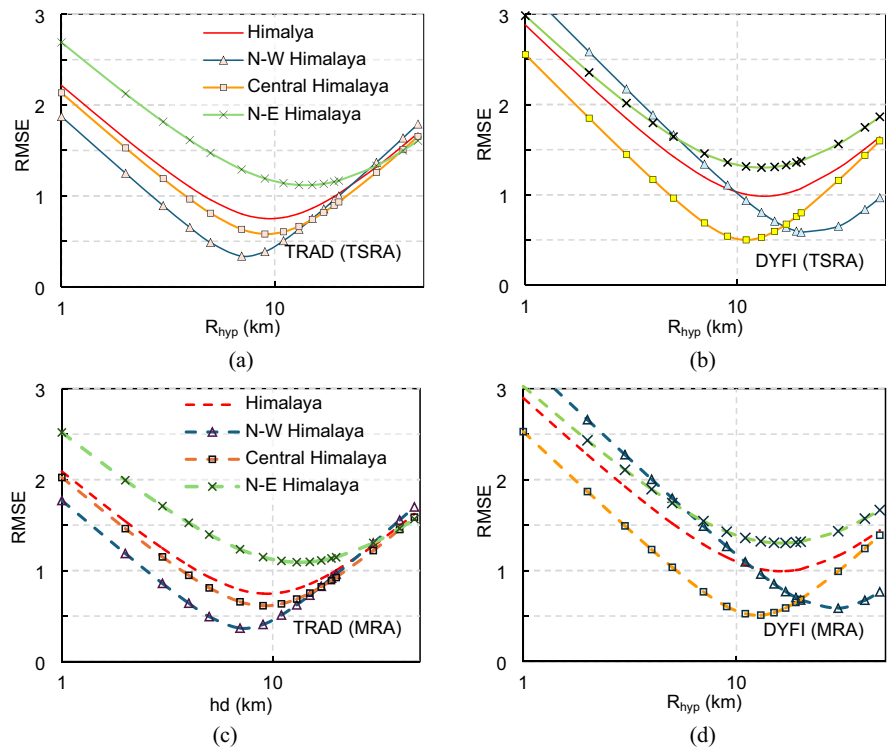
epicentral intensities by G&M11 for a hypothetical major earthquake (Mw7.0) are almost a unit higher as compared to TRAD one. In contrast, those predicted by G&M13 are a unit lower. Anelastic attenuation behaviour for G&M11 and TRAD is almost similar and has a pronounced effect at far-site distances (> 200 km). In contrast, for G&M13, it is almost negligible. DYFI's predicted IPEs for M_w 5.0 show the least magnitude of geometric attenuation and almost zero effect of anelastic attenuation. For M_w 7.0, we have not drawn the DYFI's corresponding plot as it is outside the M_w limits for the IPE and gives erroneous results.

4.5 IPE for Central and North-East (N-E) Himalaya

IPEs obtained from TSRA results for the TRAD and DYFI dataset (as per events in Table 4 for Central Himalaya) are

$$I(\text{TRAD}) = 0.70 + 1.63M - 0.046M^2 - 0.0013R_{hyp} - 0.84\ln\left(R_{hyp}\right)$$

$$\text{here } M \in \begin{cases} 4.6 \le M_w \le 7.8 \text{ if } M = M_w \\ 4.2 \le M_{wg} \le 7.7 \text{ if } M = M_{wg} \end{cases},$$

$$R^2 = 0.47, \sigma = 0.96; h_d = 9\text{km}$$

(14)

$$I(\text{DYFI}) = 3.19 + 1.27M - 0.036M^2 - 0.00017R_{hyp} - 1.06\ln\left(R_{hyp}\right)$$

$$\text{here } M \in \begin{cases} 4.6 \le M_w \le 7.8 \text{ if } M = M_w \\ 4.2 \le M_{wg} \le 7.7 \text{ if } M = M_{wg} \end{cases},$$

$$R^2 = 0.32, \sigma = 1.12; h_d = 11\text{km}$$

(15)

N-E Himalayan region IPEs from MRA and TSRA results for TRAD and DYFI datasets (prepared for the earthquake listed in Table 4 for N-E Himalaya), respectively, are

$$I(\text{TRAD}) = 3.58 + 1.37M - 0.058M^2 - 0.0008R_{hyp} - 0.92\ln\left(R_{hyp}\right)$$

$$\text{here } M \in \begin{cases} 5.6 \le M_w \le 8.6 \text{ if } M = M_w \\ 5.3 \le M_{wg} \le 8.6 \text{ if } M = M_{wg} \end{cases},$$

$$R^2 = 0.58, \sigma = 0.91; h_d = 13\text{km}$$

(16)

$$I(\text{DYFI}) = -6.96 + 5.00M - 0.34M^2 + 0.00079R_{hyp} - 1.33\ln\left(R_{hyp}\right)$$

$$\text{here } M \in \begin{cases} 5.4 \le M_w \le 6.7 \text{ if } M = M_w \\ 5.1 \le M_{wg} \le 6.5 \text{ if } M = M_{wg} \end{cases},$$

$$R^2 = 0.31, \sigma = 1.07; h_d = 13\text{km}$$

(17)

Residual plots for Eqs. (14)–(17) against R_{hyp} are shown in Fig. 9, along with the mean and standard deviation of residuals indicated with error bars. Mean

Fig. 7 Variation of residuals, i.e., (observed intensity)–(predicted intensity) or (I_{obs}–I_{pred}) w.r.t the hypocentral distance, R_{hyp} for Himalaya (**a, b**), N-W Himalaya in (**c, d**), using TRAD (circles) and DYFI (squares) datasets, respectively. Error bars represent the standard deviation for a given distance bin. A linear fit between residuals ($\varepsilon = I_{obs} - I_{pred}$) and R_{hyp} with functional form: $\varepsilon = \alpha \ln(R) + \beta$ has also been plotted


(a)

(b)

(c)

(d)
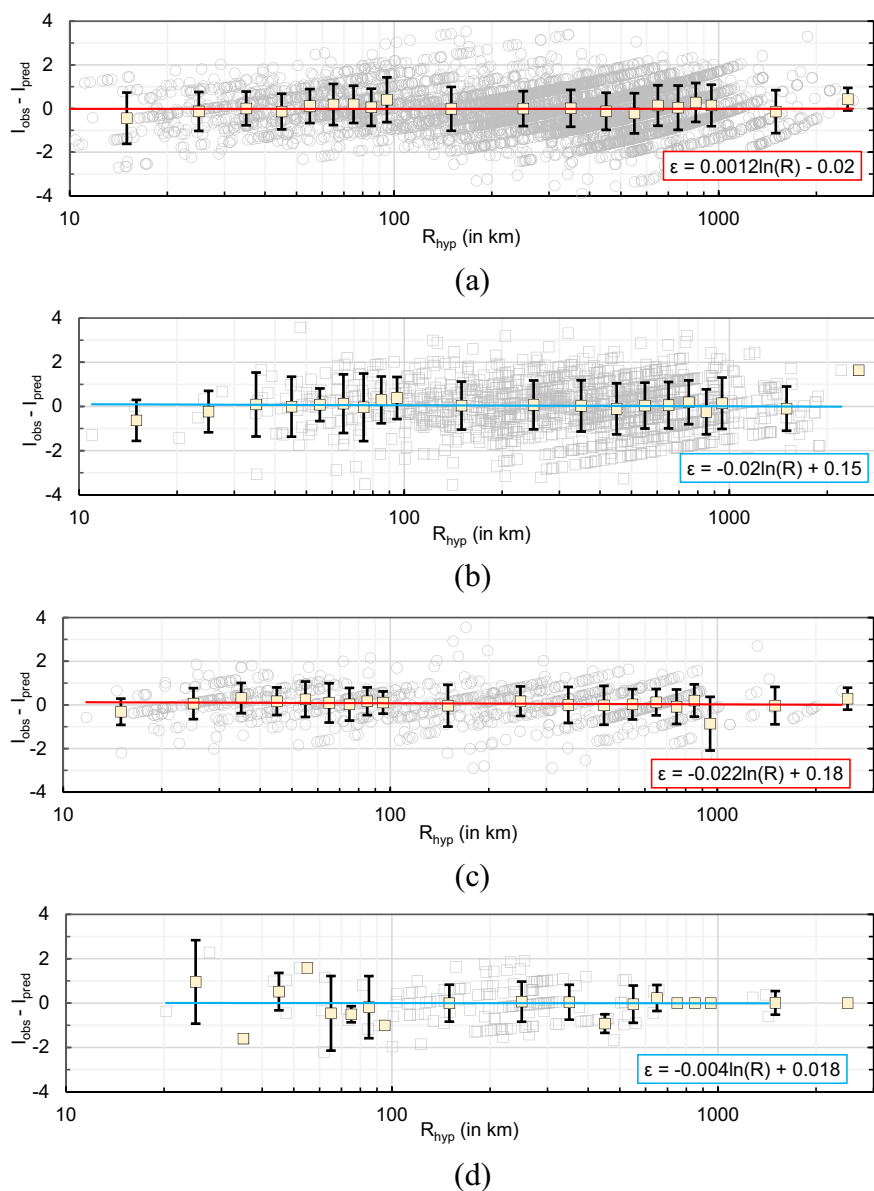
values for a particular distance bin are generally closer to zero over the range of R_{hyp} values, except for near-site distances (< 30 km) for the TRAD Central Himalayas, where intensities are overpredicted. An approach like Allen et al. (2012) for IPEs or by Bajaj and Anbazhagan (2018) for GMPEs may be used to resolve these issues by developing separate IPEs for different distance metric ranges (e.g., near- or far-site) or magnitude ranges for same regions.
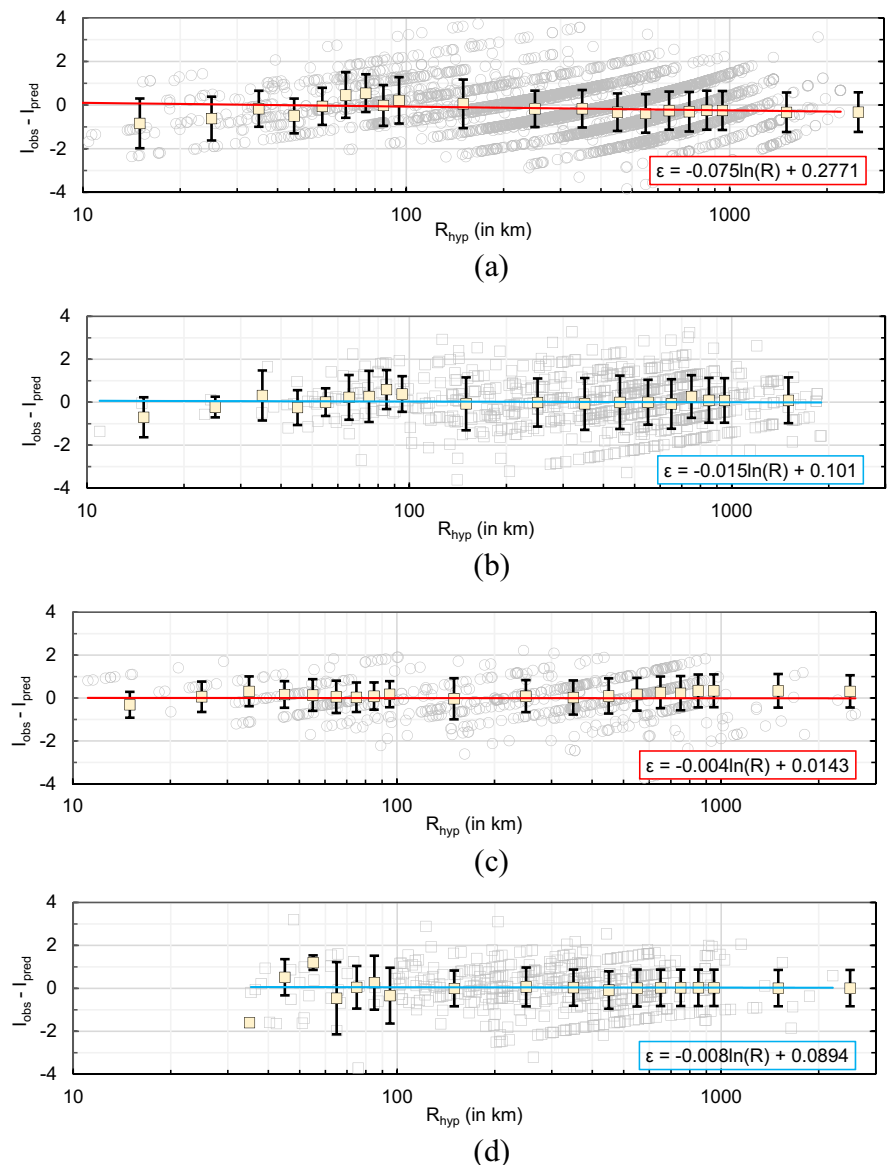
But, in our dataset for Central Himalaya, the number of IDPs in these distance ranges is too low to produce any significant advantage for the intensity prediction. DYFI residuals for these regions also show this pattern due to a small number of IDPs at this R_{hyp} range. Standard deviation values for the DYFI residuals over the bins are consistently higher than their TRAD counterpart (Fig. 9).

Prajapati et al. (2013) have given IPE applicable for Sikkim Himalaya (Table 1) by using five events, four

Fig. 8 Intensity vs. R_{epi} plots for hypothetical events of magnitude **a** M_w 5.0 and **b** M_w 7.0 in N-W Himalaya using different IPEs developed for the region. G&M11 and G&M13 were used after applying Das et al. (2011) relation for conversion between M_s and M_w. TRAD: Eq. (12); DYFI: Eq. (13)


(a)

(b)
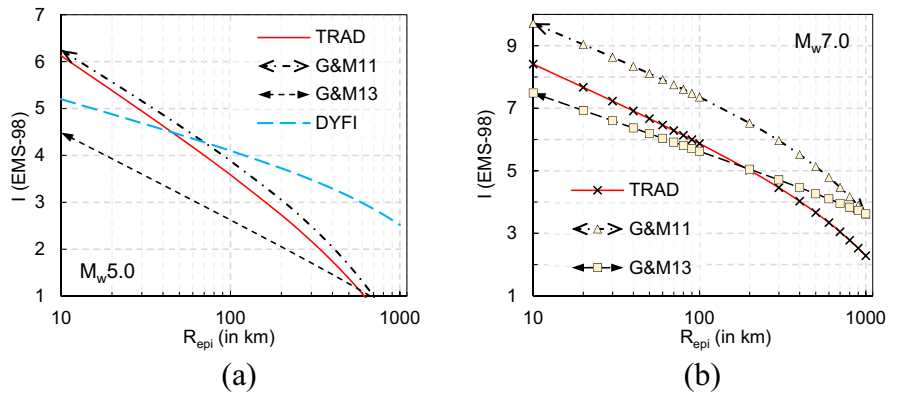
Fig. 9 Variation of residuals, i.e., (observed intensity)–(predicted intensity) or ($I_{obs}-I_{pred}$) w.r.t. the hypocentral distance, R_{hyp} for Central Himalaya in **a** and **b**, and N-E Himalaya in **c** and **d** using TRAD (circles) and DYFI (squares) datasets, respectively. Error bars represent the standard deviation for a given distance bin. A linear fit between residuals (ε) and R_{hyp} with functional form: $\varepsilon = \alpha \ln(R) + \beta$ has also been plotted

$\varepsilon = -0.075\ln(R) + 0.2771$

(a)

$\varepsilon = -0.015\ln(R) + 0.101$

(b)

$\varepsilon = -0.004\ln(R) + 0.0143$

(c)

$\varepsilon = -0.008\ln(R) + 0.0894$

(d)

Fig. 10 Intensity variation w.r.t. distance for the Himalayan region obtained using different IPEs developed for the area, for **a** M_w5.0; **c** M_w6.0; **e** M_w7.0; and **g** M_w8.0 hypothetical earthquakes. TRAD: Eq. (10); DYFI: Eq. (11); A&D04: Ambraseys and Douglas (2004); Sze10: Szeliga et al. (2010); Allen12: Allen et al. (2012)
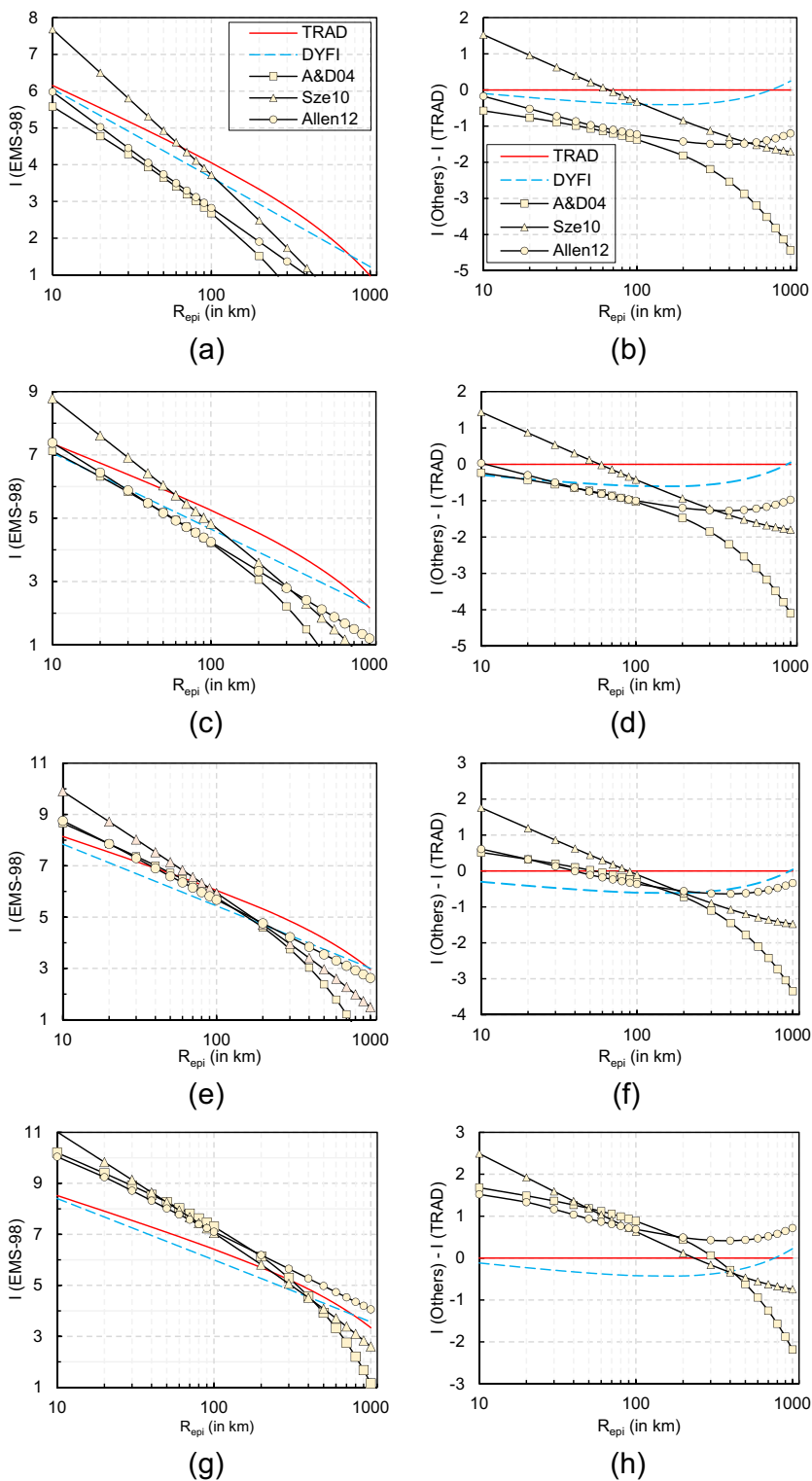
Fig. 11 Intensity variation w.r.t. distance for the sub-regions of Himalaya obtained using different IPEs, for **a, b** M_w 5.0; **c, d** M_w 6.0; **e, f** M_w 7.0; and **g, h** M_w 8.0 hypothetical earthquakes
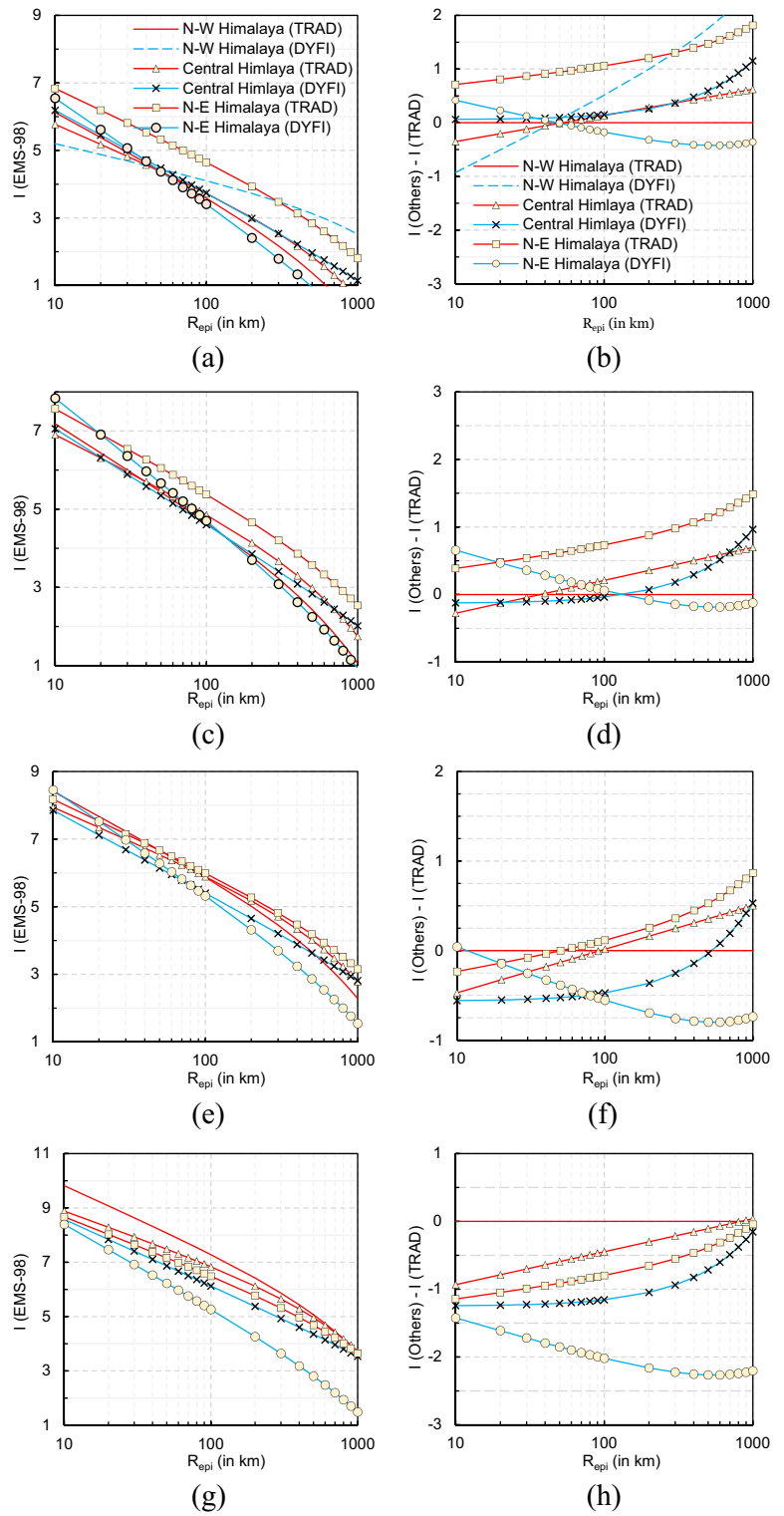
of which lie in the Central Himalayan region (including SIKKIM-2011), as per our criteria. The fifth event they have used is ASSAM-1950, which we have included in our North-East Himalaya dataset. From the IPE they reported, we have found that the intensity predicted by their IPE gives erroneous results, possibly due to unusual regression coefficient values reported.

4.6 Comparison of IPEs with past studies

Ambraseys and Douglas (2004) and Szeliga et al. (2010) have developed IPEs for the whole Himalayan region based on data from traditional sources. Allen et al. (2012) have developed IPEs (for M_w 5.0–7.9 and $R_{hyp} \leq 300$ km) for active crustal areas (which also include the Himalayas) using global macroseismic Intensity observations (13,077 IDPs) collected from traditional and DYFI reports. They have developed separate IPEs based on the IDP's distance from the fault rupture (R_{rup}) and R_{hyp} metrics. Their functional form of IPEs differs slightly from those given in Eqs. (1) and (2). For comparison with our IPEs, we have used the IPE given by Allen et al. (2012) for R_{hyp} (hereafter referred to as Allen12). They have highlighted the overestimation issues of IPEs for near-site distances. In comparison to TRAD IPE (Eq. 10), A&D04 shows higher anelastic attenuation over the far-site distances (> 100 km) for different earthquake magnitudes (Fig. 10), whereas for Sze10, Allen12 and DYFI, this effect is negligible. For near-site distances,

Intensity attenuation due to geometric spreading is highest in Sze10, followed by (in order) Allen12, A&D04, and DYFI. A&D04 and Sze10 predict epicentral intensities (I_0) 1–2 units higher (for M_w 8.0) than TRAD and DYFI.

For lower magnitude (M_w 6.0), I_0 expected by A&D04 and DYFI matches, whereas those indicated by Sze10 are almost a unit higher. Allen et al. (2012) have mentioned that their IPEs underestimate the intensity for M_w 5.0–5.5, the possible cause of which is the lack of low-intensity IDPs at far-site distances. The scaling of I_0 w.r.t. M_w has the highest magnitude for A&D10 and the lowest for the DYFI dataset. The difference in predicted TRAD and DYFI intensities remains almost the same (< 0.5 Intensity units) for the entire M_w (5–8) range.

If we compare the IPEs developed for sub-regions of the Himalayas (Fig. 11), for lower magnitudes (M_w 5.0 and M_w 6.0), Intensities predicted by N-E Himalayan TRAD IPE (Eq. 16) are consistently higher as compared to the other two regions between M_w 5.0–7.0. Attenuation due to geometric spreading is slightly higher (Fig. 11) for N-W Himalaya than the other two areas for TRAD-based IPEs. The effect of anelastic attenuation for TRAD IPEs is the same for N-W and Central Himalaya, in which a near-parallel drop in predicted intensities (at far-site distances) can be observed.

DYFI-based IPE for N-W Himalaya (Eq. (13)) and N-E Himalaya (Eq. (17)) show a considerable deviation in Fig. 11 from those predicted by

Table 8 Events considered to check the suitability of prediction equations. ComCat EventID given in the table will be used as "EVENTID" at the following web address: http://earthquake.usgs.gov/earthquakes/eventpage/EVENTID

S. No	Event		Epicentre		M_w	Focal depth (km)	I_{max}	IDPs	Scale	ComCat EventID
	Date	Designation	Lat (°N)	Long (°E)						
1a	12 May 2015	DOLAKHA-2015 (TRAD)	27.81	86.07	7.3	15.0	8	1263	EMS-98	-
1b	12 May 2015	DOLAKHA-2015 (DYFI)	27.81	86.07	7.3	15.0	8	261	MMI	us20002ejl
2	05 Apr 2021	BHUTAN-2021	27.19	88.94	5.5*	10.0	6	63		us6000dz5d
3	25 Nov 2021	MYANMAR-2021	22.82	93.51	6.2	43	8	97		us7000fx45
4	31 Jul 2022	NEPAL-2022A	27.13	86.78	5.3*	10.0	6	30		us6000i6vr
5	08 Nov 2022	NEPAL-2022B	29.29	81.16	5.7	11.0	8	137		us7000incn
6	24 Jan 2023	NEPAL-2023	29.58	81.66	5.4	33.1	7	28		us6000jivm
7	13 Jun 2023	JAMMU-2023	33.12	75.91	5.2	10.0	7	39		us7000k850
8	16 Jun 2023	BANGLADESH-2023	24.73	92.02	5.2*	10.0	6	24		us7000k8uw
9	14 Aug 2023	ASSAM-2023	24.98	92.25	5.3	36.6	6	47		us6000kzvl

M_w moment magnitude, I_{max} maximum intensity, *IDP* Intensity Data Point

*M_w obtained after using Das et al. (2011) relationship between M_w and mb

Table 9 LLH values calculated for the different events using TRAD and DYFI equations applicable for whole, N-W, Central, and N-E Himalayan regions (minimum values are underlined). LLH values in rows corresponding to TRAD (columns 2–5) have been calculated from Eq. 10, Eq. (12), Eq. (14), and Eq. (16), and for DYFI rows (columns 2–5) using Eq. (11), Eq. (13), Eq. (15), and Eq. (17). Here, N-W–North-Western Himalaya, N-E–North-Eastern Himalaya. Note: Except DOLAKHA-2015 all other events data is of DYFI type

| IPE	Region			
	Whole (Col. 2)	N-W (Col. 3)	Central (Col. 4)	N-E (Col.5)
DOLAKHA-2015 (TRAD)				
TRAD	1.915	2.280	1.916	1.886
DYFI	1.937	1333.8	1.898	3.210
DOLAKHA-2015 (DYFI)				
TRAD	4.017	4.622	4.066	4.084
DYFI	2.864	1410.6	2.832	2.832
BHUTAN-2021				
TRAD	2.800	4.272	2.823	3.328
DYFI	2.220	3.054	2.282	2.276
MYANMAR-2021				
TRAD	3.448	5.145	3.495	3.411
DYFI	3.016	30.270	2.905	2.936
NEPAL-2022A				
TRAD	4.434	3.767	4.666	6.767
DYFI	2.832	3.248	2.760	2.619
NEPAL-2022B				
TRAD	2.507	4.708	2.475	2.446
DYFI	2.308	2.683	2.351	2.232
NEPAL-2023				
TRAD	2.303	3.820	2.328	2.591
DYFI	2.104	3.736	2.152	2.143
JAMMU-2023				
TRAD	3.245	4.599	3.297	3.903
DYFI	2.449	3.210	2.500	2.494
BANGLADESH-2023				
TRAD	2.821	2.821	2.957	4.146
DYFI	2.320	3.808	2.232	2.264
ASSAM-2023				
TRAD	3.306	4.464	3.358	3.875
DYFI	2.644	4.464	2.649	2.705

corresponding TRAD-based IPEs (Eqs. (12) and (16)). This is due to the limited magnitude range of applicability for both IPEs compared to their TRAD-based counterparts. Hence, we would recommend considering the M_w (or M_{wg}) range while using these IPEs. The Central Himalayan IPEs (Eqs. (14) and (15)) predict similar intensities for M_w 5.0–7.0, but a deviation (positive or negative) of the approximately half-intensity unit can be observed (Fig. 11). At M_w 8.0, N-W TRAD IPE predicted consistently higher Intensities than all other IPEs, possibly due to the type of building infrastructure in these regions.

The coefficient of the M_w^2 term is negative for all other IPEs Eqs. (10)–(17) except for Eqs. (12) and (13) N-W Himalaya IPEs, which is as expected because intensity values should saturate over higher M_w values as the observed effects defined for higher intensities are infrastructure dependent (Atkinson and Boore 2003; Musson 2005). But like Atkinson and Boore (2003) and Musson (2005), the coefficients for N-W Himalaya are positive. Atkinson and Boore (2003) have avoided this issue by refitting the quadratic functional form with an equivalent linear fit, whereas Musson (2005) has justified it based on the explanation given by Fukushima (1996). Fukushima (1996) highlighted that a positive coefficient for M_w^2 can be observed for the predictions based on the Richter scale (M_L) due to the difference in magnitude scaling w.r.t. seismic moment. We have not changed Eq. (12) over its applicable range because the predicted I vs. M_w relation is almost linear, whereas for Eq. (13), the improvement in the model by including M_w^2 is significant compared to a linear one and the applicable M_w range is small such that the positive coefficient would not highly exaggerate the predicted intensities.

4.7 A check for IPE performance

To assess how the newly developed IPEs perform, we have utilized DYFI data from the USGS website for the

Fig. 12 TRAD and DYFI intensities reported for the Dolakha 2015 event, along with predicted intensities as per TRAD and DYFI-based IPEs (Eqs. (10) and (11)) applicable for the Himalayan region
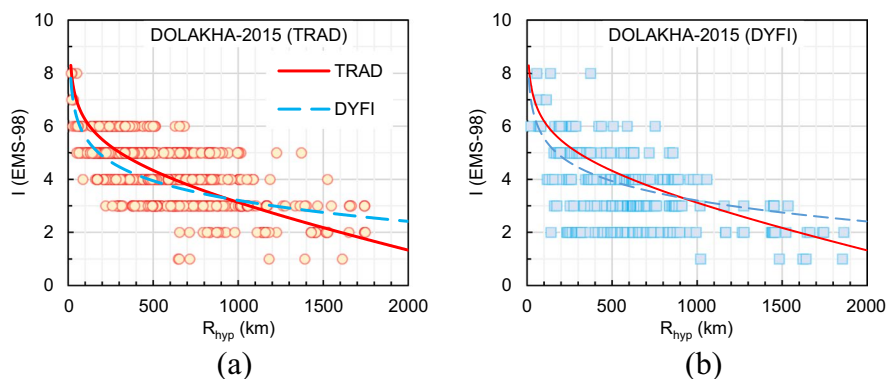
earthquakes occurring between 2021 and 2023, which were not included in the IPEs' development and had a significant number of reports (Table 8). We have also considered TRAD and DYFI data available for the 2015 Dolakha, Nepal M_w 7.3 magnitude (hereafter DOLAKHA-2015) earthquake to compare the performance of IPEs and their applicability to the datasets. TRAD data for this event with 1473 IDPs reported have been used from Hough et al. (2016). After reassessing these values according to the earlier criteria, our final dataset has 1263 IDPs for this event. Calculated LLH values are given in Table 9 for the events not considered in the IPE development. These values imply that for all the events, TRAD and DYFI-based IPEs applicable for the whole of the Himalayas are more suitable for their respective data types' intensity prediction than their counterparts, as indicated by lower LLH values. In a few cases, the DYFI-based IPE developed for N-W Himalaya has given very high LLH values due to very few events (only 3) considered for the IPE development.

These higher LLH values also highlight the potential pitfall of using past IPEs based on a small number of events. Figures 12 and 13 show the plot of macroseismic intensity values reported (TRAD and DYFI) for the events listed in Table 8, along with the variation of predicted intensity based on the IPEs developed in this study.

5 Conclusion

We have used Intensity values reported for earthquakes between 1950 and 2020 from traditional sources (like field surveys, media reports, and newspapers) or TRAD and between 2011 and 2021 from USGS DYFI's online database to develop IPEs for the Himalayas and its

sub-regions. For IPE development, we have used two different regression techniques: one-stage multiple regression and two-stage regression (while incorporating a first- and second-order magnitude fit). Still, there was not much difference in their performance for the Intensity prediction. First and second-order intensity vs. magnitude relationships were used in IPEs development. We have developed IPEs based on the moment magnitude scale (M_w) and generalized moment magnitude scale, M_{wg} (or Das magnitude scale), also given applicable range equations for in both M_w and M_{wg}. We also provided conversion equations between M_w and M_{wg}.

A concept of optimal hypocentral depth has also been proposed in the study, which corresponds to a minimum hypocentral depth value that minimizes root-mean-squared error in such a way that the proposed IPEs correspond to a best-fit I_{max} vs M_w relationship for this distance. The calculated optimal depth can be used to get the maximum value of macroseismic Intensity for a particular earthquake. This optimal depth criterion has been used to select applicable relations from the IPEs developed using two regression methods (and different magnitude orders) for the different regions of the Himalayas.

These newly developed IPEs can be used to assess the hazard and risk of future earthquakes in the region. Separate IPEs for sub-regions of Himalaya were also developed to segregate the effects of source and site characteristics depending upon the area. These can be useful for hazard assessment at a micro-level. A comparison of IPEs developed from TRAD and DYFI data indicates that DYFI-based predicted intensities are consistently lesser than their TRAD counterpart. This highlights a major difference

Fig. 13 DYFI intensities and predicted intensities values for the events not considered in the dataset for regression. Predicted intensities were calculated for the different events using TRAD and DYFI IPEs (Eqs. (10) and (11)) applicable to the Himalayan region

(a)

(b)

(c)

(d)

(e)

(f)

(g)
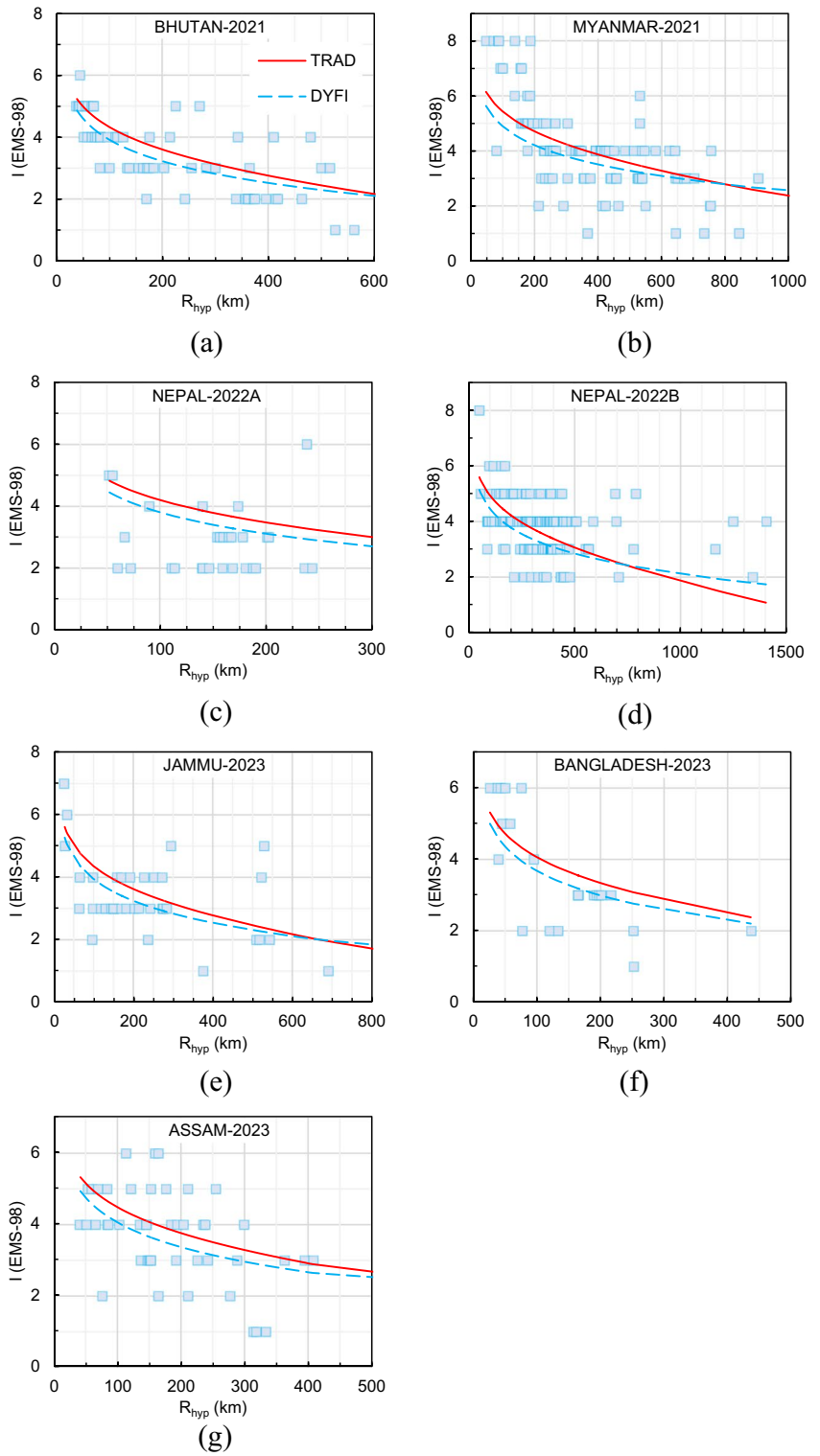
between the two types of macroseismic data, which can be researched further. Comparison of the IPEs based on the Log-Likelihood method results for the events not considered in IPE development highlights the importance of developing separate IPEs for the TRAD and DYFI data collection methods. IPEs presented here have error terms, which can be further used for probabilistic intensity mapping.

Author contribution   Both authors contributed to the conceptualization of the study. H.T. contributed to the data collection, analysis, and writing of the first draft. A.P. contributed to supervising, reviewing, and editing the manuscript.

Data availability   No datasets were generated or analysed during the current study.

Declarations

Competing interests   The authors declare that they have no competing financial interests or personal relationships that could have appeared to influence the work reported in this paper.

References

Ahmadzadeh S, Doloei GJ, Zafarani H (2020) New Intensity Prediction Equation for Iran. J Seismol 24:23–35. https://doi.org/10.1007/s10950-019-09882-7

Allen TI, Wald DJ, Worden CB (2012) Intensity attenuation for active crustal regions. J Seismol 16:409–433. https://doi.org/10.1007/s10950-012-9278-7

Allen TI, Wald DJ, Hotovec AJ, Lin K, Earle PS, Marano KD (2008) An Atlas of ShakeMaps for Selected Global Earthquakes. U.S. Geological Survey Open-File Report 2008–1236, p 35

Alpyürür M, Lav MA (2022) An assessment of probabilistic seismic hazard for the cities in Southwest Turkey using historical and instrumental earthquake catalogs. Nat Hazards 114(1):335–365. https://doi.org/10.1007/s11069-022-05392-x

Ambraseys NN (2001) Reassessment of earthquakes, 1900–1999, in the Eastern Mediterranean and the Middle East. Geophys J Int 145(2):471–485. https://doi.org/10.1046/j.0956-540x.2001.01396.x

Ambraseys NN, Douglas J (2004) Magnitude calibration of north Indian earthquakes. Geophys J Int 159:165–206. https://doi.org/10.1111/j.1365-246X.2004.02323.x

Anbazhagan P, Bajaj K, Matharu K, Moustafa SS, Al-Arifi NS (2019) Probabilistic seismic hazard analysis using logic tree approach - Patna District (India). Nat Hazards Earth Syst Sci 19:2097–2115. https://doi.org/10.5194/nhess-19-2097-2019

Anbazhagan P, Sreenivas M, Ketan B, Moustafa SSR, Al-Arifi NS (2016) Selection of ground motion prediction equations for seismic hazard analysis of peninsular India. J Earthq Eng 20(5):699–737. https://doi.org/10.1080/13632469.2015.1104747

Atkinson GM, Boore DM (2003) Empirical ground-motion relations for subduction-zone earthquakes and their application to Cascadia and other regions. Bull Seism Soc Am 93(4):1703–1729. https://doi.org/10.1785/0120020156

Atkinson GM, Wald DJ (2007) "Did You Feel It?" intensity data: a surprisingly good measure of earthquake ground motion. Seism Res Lett 78:362–368. https://doi.org/10.1785/gssrl.78.3.362

Atkinson GM, Worden CB, Wald DJ (2014) Intensity Prediction Equations for North America. Bull Seism Soc Am 104(6):3084–3093. https://doi.org/10.1785/0120140178

Bajaj K, Anbazhagan P (2018) Determination of GMPE functional form for an active region with limited strong motion data: application to the Himalayan region. J Seismol 22:161–185. https://doi.org/10.1007/s10950-017-9698-5

Bajaj K, Anbazhagan P (2019) Regional stochastic GMPE with available recorded data for active region–application to the Himalayan region. Soil Dyn Earthq Eng 126:105825. https://doi.org/10.1016/j.soildyn.2019.105825

Bakun WH, Scotti O (2006) Regional intensity attenuation models for France and the estimation of magnitude and location of historical earthquakes. Geophys J Int 164(3):596–610. https://doi.org/10.1111/j.1365-246X.2005.02808.x

Baumont D, Manchuel K, Traversa P, Durouchoux C, Nayman E, Ameri G (2018) Intensity predictive attenuation models calibrated in Mw for metropolitan France. Bull Earthq Eng 16:2285–2310. https://doi.org/10.1007/s10518-018-0344-6

Bayrak E, Nas M, Bayrak Y (2019) New macroseismic intensity predictive models for Turkey. Acta Geophys 67:1483–1513. https://doi.org/10.1007/s11600-019-00357-4

Beauval C, Tasan H, Laurendeau A, Delavaud E, Cotton F, Guéguen P, Kuehn N (2012) On the testing of ground-motion prediction equations against small-magnitude data. Bull Seismol Soc Am 102(5):1994–2007. https://doi.org/10.1785/0120110271

Bharali B, Rakshit R, Dinpuia L, Saikia S, Baruah S (2021) The 2020 Mw 5.5 Mizoram earthquake and associated swarm activity in the junction of the Surma Basin and Indo-Myanmar Subduction Region. Nat Hazards 109:2381–2398. https://doi.org/10.1007/s11069-021-04924-1

BMTPC (2019) Vulnerability Atlas of India: 3rd edition, Ministry of Housing and Urban Affairs, Government of India, India. https://vai.bmtpc.org/

Boore DM, Joyner WB (1982) The empirical prediction of ground motion. Bull Seism Soc Am 72(6B):S43–S60. https://doi.org/10.1785/BSSA07206B0043

Boore DM, Joyner WB, Fumal TE (1993) Estimation of response spectra and peak accelerations from western North America earthquakes: an interim report, Open-File-Report 93–509, US Geological Survey, Reston, Virginia, 72

Chandra U (1980) Attenuation of intensities in India. In: Proceedings of the 7th World Conference on Earthquake Engineering, vol 2. Istanbul, Turkey, pp 521–524

Cramer CH (2020) Updated GMICE for Central and Eastern North America Extending to Higher Intensities. Seism Res Lett 91(6):3518–3527. https://doi.org/10.1785/0220200061

Das R, Wason HR, Sharma ML (2011) Global regression relations for conversion of surface wave and body wave magnitudes to moment magnitude. Nat Hazards 59:801–810. https://doi.org/10.1007/s11069-011-9796-6

Das R, Sharma ML, Wason HR, Choudhury D, Gonzalez G (2019) A seismic moment magnitude scale. Bull Seismol Soc Am 109(4):1542–1555. https://doi.org/10.1785/0120180338

Das R, Menesis C, Urrutia D (2023) Regression relationships for conversion of body wave and surface wave magnitudes toward Das magnitude scale. MWg Natural Hazards 117(1):365–380. https://doi.org/10.1007/s11069-023-05863-9

Debbarma J, Martin SS, Suresh G, Ahsan A, Gahalaut VK (2017) Preliminary observations from the 3 Jan 2017, MW 5.6 Manu, Tripura (India) earthquake. Journal of Asian Earth Sciences 148:173–180. https://doi.org/10.1016/j.jseaes.2017.08.030

Delavaud E, Scherbaum F, Kuehn N, Allen T (2012) Testing the global applicability of ground-motion prediction equations for active shallow crustal regions. Bulletin of the Seismological Society of America 102(2):707–721. https://doi.org/10.1785/0120110113

Dolce M, Masi A, Marino M, Vona M (2003) Earthquake damage scenarios of the building stock of Potenza (Southern Italy) including site effects. Bull Earthq Eng 1:115–140. https://doi.org/10.1023/A:1024809511362

Du K, Ding B, Luo H, Sun J (2018) Relationship between peak ground acceleration, peak ground velocity, and macroseismic intensity in Western China. Bull Seism Soc Am 109(1):284–297. https://doi.org/10.1785/0120180216

Engdahl ER, Villasenor A (2002) Global seismicity: 1900–1999, in International Handbook of Earthquake and Engineering Seismology, Lee WHK, Kanamori H, Jennings PC, Kisslinger C (Editors), Vol. A, chap. 41, Academic Press, Boston, 665–690. https://doi.org/10.1016/S0074-6142(02)80244-3

Fukushima Y (1996) Scaling relations for strong ground motion prediction models with M 2 terms. Bull Seism Soc Am 86(2):329–336. https://doi.org/10.1785/BSSA0860020329

Gahalaut VK, Martin SS, Srinagesh D, Kapil SL, Suresh G, Saikia S, Kumar V, Dadhich H, Patel A, Prajapati SK, Shukla HP, Gautam JL, Baidya PR, Mandal S, Jain A (2016) Seismological, geodetic, macroseismic and historical context of the 2016 Mw 6.7 Tamenglong (Manipur) India earthquake. Tectonophysics 688:36–48. https://doi.org/10.1016/j.tecto.2016.09.017

Gasperini P (2001) The attenuation of seismic Intensity in Italy: a bilinear shape indicates the dominance of deep phases at epicentral distances longer than 45 km. Bull Seismol Soc Am 91(4):826–841. https://doi.org/10.1785/0120000066

Geli L, Bard PY, Jullien B (1988) The effect of topography on earthquake ground motion: a review and new results. Bull Seism Soc Am 78(1):42–63. https://doi.org/10.1785/BSSA0780010042

Ghosh GK, Mahajan AK (2011) Interpretation of Intensity Attenuation Relation of 1905 Kangra Earthquake with Epicentral Distance and Magnitude in the Northwest Himalayan Region. J Geol Soc India 77:511–520. https://doi.org/10.1007/s12594-011-0058-8

Ghosh GK, Mahajan AK (2013) Intensity attenuation relation at Chamba-Garhwal area in north-west Himalaya with epicentral distance and magnitude. J Earth Syst Sc 122:107–122. https://doi.org/10.1007/s12040-012-0261-z

Goda K, Kiyota T, Pokhrel RM, Chiaro G, Katagiri T, Sharma K, Wilkinson S (2015) The 2015 Gorkha Nepal earthquake: insights from earthquake damage survey. Front Built Environ 1:8. https://doi.org/10.3389/fbuil.2015.00008

Gomez-Capera AA, Santulin M, D'Amico M, D'Amico V, Locati M, Meletti C and Varini E (2023) Macroseismic intensity attenuation models calibrated in Mw for Italy. Bullet Earthq Eng 1–49. https://doi.org/10.1007/s10518-023-01822-8

Grunthal G, Leveret A (eds) (1998) European macroseismic scale 1998 (EMS-98). Cahiers du Centre Européen de Géodynamique et de Séismologie, Luxembourg, p 15. https://doi.org/10.2312/EMS-98.full.en

Gupta HK, Rastogi BK, Mohan I, Rao CVRK, Sarma SVS, Rao RUM (1998) An investigation into the Latur earthquake of September 29, 1993 in southern India. Tectonophysics 287(1-4):299–318. https://doi.org/10.1016/S0040-1951(98)80075-9

Gupta AK, Chopra S, Prajapati SK, Sutar AK, Bansal BK (2013) Intensity distribution of M 4.9 Haryana–Delhi border earthquake. Nat Hazards 68:405–417. https://doi.org/10.1007/s11069-013-0638-6

Hanks TC, Kanamori H (1979) A moment magnitude scale. Journal of Geophysical Research: Solid Earth 84(B5):2348–2350

Hough SE, Martin SS (2021) Which earthquake accounts matter? Seism Res Lett 92(2A):1069–1084. https://doi.org/10.1785/0220200366

Hough SE, Martin SS, Gahalaut V, Joshi A, Landes M, Bossu R (2016) A comparison of observed and predicted ground motions from the 2015 Mw 7.8 Gorkha, Nepal, earthquake. Nat Hazards 84:1661–1684. https://doi.org/10.1007/s11069-016-2505-8

Howell BF, Schultz TR (1975) Attenuation of modified mercalli intensity with distance from the epicenter. Bull Seism Soc Am 65(3):651–665. https://doi.org/10.1785/BSSA0650030651

Jaiswal K, DJ Wald, M Hearne (2009) Estimating casualties for large earthquakes worldwide using an empirical approach: US Geological Survey Open-File Report of 2009–1136, 78. https://doi.org/10.3133/ofr20091136

Joyner WB, Boore DM (1981) Peak horizontal acceleration and velocity from strong-motion records including records from the 1979 Imperial Valley, California, earthquake; Bulletin of the Seismological Society of America 71(6):2011–2038. https://doi.org/10.1785/BSSA0710062011

Kaiser A, Holden C, Massey C (2013) Determination of site amplification, polarization and topographic effects in the seismic response of the Port Hills following the 2011 Christchurch earthquake. In NZSEE Conference, Wellington, New Zealand (1–8). http://www.nzsee.org.nz/db/2013/Poster_10.pdf

Kayal JR (2008) Microearthquake seismology and seismotectonics of South Asia. Springer Science & Business Media. https://doi.org/10.1007/978-1-4020-8180-4

Martin SS, Hough SE (2015) The 21 May 2014 M w 5.9 Bay of Bengal earthquake: macroseismic data suggest a high-stress-drop event. Seism Res Lett 86(2A):369–377. https://doi.org/10.1785/0220140155

Martin S, Szeliga W (2010) A catalog of felt intensity data for 570 earthquakes in India from 1636 to 2009. Bull Seism Soc Am 100(2):562–569. https://doi.org/10.1785/0120080328

Martin SS, Hough SE, Hung C (2015) Ground Motions from the 2015 Mw 7.8 Gorkha, Nepal, Earthquake Constrained by a Detailed Assessment of Macroseismic Data, Seismological Research Letters 86(6):1524–1532. https://doi.org/10.1785/0220150138

Mucciarelli M, Peruzza L, Caroli P (2000) Tuning of seismic hazard estimates by means of observed site intensities. J Earthq Eng 4(2):141–159. https://doi.org/10.1080/13632460009350366

Musson RMW (1996) Determination of parameters for historical British earthquakes. Ann Geophys 39:1041–1048. https://doi.org/10.4401/ag-4035

Musson RMW (2005) Intensity attenuation in the UK. J Seismol 9:73–86. https://doi.org/10.1007/s10950-005-2979-4

Musson RMW, Grünthal G, Stucchi M (2010) The comparison of macroseismic intensity scales. J Seismol 14:413–428. https://doi.org/10.1007/s10950-009-9172-0

Musson RMW (2013) Updated intensity attenuation for the UK. British Geological Survey Open Report, OR/13/029, p 19. https://nora.nerc.ac.uk/id/eprint/503214

Pasolini C, Gasperini P, Albarello D, Lolli B, D'Amico V (2008) The attenuation of seismic Intensity in Italy, part I: theoretical and empirical backgrounds. Bull Seismol Soc Am 98(2):682–691. https://doi.org/10.1785/0120070020

Pasolini C, Albarello D, Gasperini P, Amico VD, Lolli B (2008) The attenuation of seismic intensity in Italy, Part II: modeling and Validation. Bull Seismol Soc Am 98(2):692–708. https://doi.org/10.1785/0120070021

Pitilakis K (2004) Site effects. In: Recent advances in earthquake geotechnical engineering and microzonation. Springer Netherlands, Dordrecht, pp 139–197. https://doi.org/10.1007/1-4020-2528-9_6

Prajapati SK, Kumar A, Chopra S, Bansal BK (2013) Intensity map of Mw 6.9 2011 Sikkim-Nepal border earthquake and its relationships with PGA: distance and magnitude. Nat Hazards 69:1781–1801. https://doi.org/10.1007/s11069-013-0776-x

Rajendran K, Rajendran CP, Thulasiraman N, Andrews R, Sherpa N (2011). The 18 September 2011, North Sikkim earthquake. Current Science 101(11):1475–1479. http://www.jstor.org/stable/24080227

Rajendran K, Parameswaran RM, Rajendran CP (2017) Seismotectonic perspectives on the Himalayan arc and contiguous areas: inferences from past and recent earthquakes. Earth Sci Rev 173:1–30. https://doi.org/10.1016/j.earscirev.2017.08.003

Scherbaum F, Delavaud E, Riggelesen C (2009) Model Selection in Seismic Hazard Analysis: An Information-Theoretic Perspective; Bulletin of the Seismological Society of America 99(6):3234–3247. https://doi.org/10.1785/0120080347

Singh SK, Suresh G, Dattatrayam RS, Shukla HP, Martin S, Havskov J, Pérez-Campos X, Iglesias A (2013) The Delhi 1960 earthquake: epicentre, depth and magnitude. Current Science 105(8):1155–1165. http://www.jstor.org/stable/24098224

Singh A, Singh C, Kennett BLN (2015) A review of crust and upper mantle structure beneath the Indian subcontinent. Tectonophysics 644–645. https://doi.org/10.1016/j.tecto.2015.01.007

Socquet A, Simons W, Vigny C, McCaffrey R, Subaraya C, Sarsito D, Ambrosius B, Spakman W (2006) Microblock rotations and fault coupling in SE Asia triple junction (Sulawesi, Indonesia) from GPS and earthquake slip vector data. J Geophys Res 111:B08409. https://doi.org/10.1029/2005JB003963

Sørensen MB, Stromeyer D, Grünthal G (2009) Attenuation of macroseismic intensity: a new relation for the Marmara Sea Region, Northwest Turkey. Bull Seismol Soc Am 99(2A):538–553. https://doi.org/10.1785/0120080299

Storchak, DA, Di Giacomo D, Bondár I, Engdahl ER, Harris J, Lee WHK, Villaseñor A, Bormann P (2013). Public Release of the ISC-GEM Global Instrumental Earthquake Catalogue (1900-2009). Seism Res Lett 84(5);810–815. https://doi.org/10.1785/0220130034

Storchak DA, Di Giacomo D, Engdahl ER, Harris J, Bondár I, Lee WHK, Bormann P, Villaseñor A (2015) The ISC-GEM Global Instrumental Earthquake Catalogue (1900-2009): Introduction, Phys. Earth Planet. Int., 239:48–63. https://doi.org/10.1016/j.pepi.2014.06.009

Storetvedt KM (1990) The Tethys Sea and the Alpine-Himalayan orogenic belt; mega-elements in a new global tectonic system. Phys Earth Planet Inter 62(1–2):141–184. https://doi.org/10.1016/0031-9201(90)90198-7

Szeliga W, Hough S, Martin S, Bilham R (2010) Intensity, magnitude, location and attenuation in India for felt earthquakes since 1762. Bull Seism Soc Am 100:570–584. https://doi.org/10.1785/0120080329

Turner B, J Jenkins, R Turner, AL Parker, A Sinclair, S Davies, GP Hayes, A Villaseñor, RL Dart, AC. Tarr, KP Furlong, HM Benz (2013) Seismicity of the Earth 1900–2010 - Himalaya and Vicinity; USGS Open-File Report 2010–1083-J. https://doi.org/10.3133/ofr20101083J

Wu YM, Teng TL, Shin TC, Hsiao NC (2003) Relationship between peak ground acceleration, peak ground velocity, and intensity in Taiwan. Bull Seism Soc Am 93(1):386–396. https://doi.org/10.1785/0120020097

Yeats R (2012) Active faults of the world. Cambridge University Press. https://doi.org/10.1017/CBO9781139035644

Zare M (2017) Recent development of the earthquake strong motion-intensity catalog and intensity prediction equations for Iran. J Seismol 21:591–613. https://doi.org/10.1007/s10950-016-9622-4